Interaction Notes

Note 199

August 1974

On the Electromagnetic Field Penetration Through Apertures

B. D. Graves
T. T. Crow
C. D. Taylor
Mississippi State University
Mississippi State, MS 39762

Abstract

A numerical method is presented for determining the electromagnetic field diffracted by an aperture in an infinite conducting plate. Comparisons are made with the results of approximations valid at low frequencies and high frequencies. Calculations of the electromagnetic field components in the aperture, in the near zone of the aperture, and in the far zone of the aperture are made and are compared with available measured data. To determine the electromagnetic pulse penetration through apertures the singularity expansion method is considered. Some preliminary data are presented. Finally the penetration of the electromagnetic field through apertures into cavities is discussed.

Interaction Notes

Note 199

August 1974

On the Electromagnetic Field Penetration Through Apertures

B. D. Graves
T. T. Crow
C. D. Taylor
Mississippi State University
Mississippi State, MS 39762

Abstract

A numerical method is presented for determining the electromagnetic field diffracted by an aperture in an infinite conducting plate. Comparisons are made with the results of approximations valid at low frequencies and high frequencies. Calculations of the electromagnetic field components in the aperture, in the near zone of the aperture, and in the far zone of the aperture are made and are compared with available measured data. To determine the electromagnetic pulse penetration through apertures the singularity expansion method is considered. Some preliminary data are presented. Finally the penetration of the electromagnetic field through apertures into cavities is discussed.

CONTENTS

Section		Page
I	INTRODUCTION	6
II	ANALYSIS	9
	1. Integral Equations	9
	2. Numerical Solution by the Method of Moments	11
	3. Scattered Field Computation	21
	4. Singularity Expansion Method	23
III	NUMERICAL RESULTS	26
	1. Convergence of the Solution	26
	2. Aperture Field Distribution	31
	3. Diffracted Field in the Near Zone	35
	4. Diffracted Field in the Far Zone	44
	5. Singularity Expansion Results	54
	6. Cavity Backed Apertures	59
IV	CONCLUSIONS	60
V	REFERENCES	61

ILLUSTRATIONS

Figure		Page
1	Circular Disk with the Polarization of the Incident Field	20
2	Distribution of Current Density on a Disk of Diameter .0636λ, for Normal Incidence with N = 15	28
3	Distribution of Current Density on a Disk of Diameter .09549λ, for Normal Incidence with N = 15	29
4	Distribution of Current Density on a Disk of Diameter .10345λ, for Normal Incidence with N = 15	30
5	Distribution of Current Density on a Disk of Diameter .5λ, for Normal Incidence with N = 21	32
6	Distribution of Current Density on a Disk of Diameter 1.0λ for Normal Incidence with N = 33	33
7	Distribution of Current Density on a Disk of Diameter 3λ for Normal Incidence with N = 33	34
8	H-Plane Distribution of Electric Field Within an Aperture of .5λ in Diameter for Normal Incidence	36
9	E-Plane Distribution of Electric Field Within an Aperture of .5λ in Diameter for Normal Incidence	37
10	H-Plane Distribution of Electric Field Within an Aperture of 1λ in Diameter for Normal Incidence	38
11	E-Plane Distribution of Electric Field Within an Aperture of 1λ in Diameter for Normal Incidence	39
12	H-Plane Distribution of Electric Field Within an Aperture of 3λ in Diameter for Normal Incidence	40
13	E-Plane Distribution of Electric Field Within an Aperture of 3λ in Diameter for Normal Incidence	41
14	Distribution of the y Component of the Electric Field Penetrating an Aperture of 0.0157λ in Diameter for Normal Incidence	42
15	Distribution of the x Component of the Magnetic Field Penetrating an Aperture of 0.0157λ in Diameter for Normal Incidence	43

Figure		Page
16	Distribution of the y Component of the Electric Field Penetrating an Aperture of 0.5λ in Diameter for Normal Incidence	45
17	Distribution of the x Component of the Magnetic Field Penetrating an Aperture of 0.5λ in Diameter for Normal Incidence	46
18	Distribution of the y Component of the Electric Field Penetrating an Aperture of 1.0λ in Diameter for Normal Incidence	47
19	Distribution of the x Component of the Magnetic Field Penetrating an Aperture of 1.0λ in Diameter for Normal Incidence	48
20	Distribution of the y Component of the Electric Field Penetrating an Aperture of 3.0λ in Diameter for Normal Incidence	49
21	Distribution of the x Component of the Magnetic Field Penetrating an Aperture of 3.0λ in Diameter for Normal Incidence	50
22	Distribution of the y Component of the Electric Field Penetrating an Aperture of 0.5λ Diameter for Normal Incidence	51
23	Distribution of the y Component of the Electric Field Penetrating an Aperture of 1.0λ Diameter for Normal Incidence	52
24	Distribution of the y Component of the Electric Field Penetrating an Aperture of 3.0λ Diameter for Normal Incidence	53
25	Real Part of Mode Vectors Corresponding to J_r	56
26	Real Part of Mode Vectors Corresponding to J_ϕ	57
27	Real Part of Electric and Magnetic Field Natural Mode Vectors Corresponding to Poles S_{11} and S_{12}	58

TABLES

Table		Page
1	Variation of Current Density Versus Number of Zones on a Disk of Diameter 0.03183λ with Normal Incidence	27
2	Natural Frequencies for the Disk	55
3	S_{11} Versus Number of Current Zones	55

SECTION I

INTRODUCTION

The electromagnetic field penetrating an aperture in a conducting surface depends upon a number of things--the geometrical configuration of the conducting surface, the shape of the aperture, the size of the aperture, the region behind the aperture (e.g. whether it is a closed region or open region), etc. With this myriad of factors determining the field penetration it is extremely difficult to provide the ordnance engineer with an assessment of the degradation of an electromagnetic shield due to the presence of an aperture, whether it be inadvertent or deliberate. However, at low frequency the factors determining the field penetration are well understood (ref. 1). Although in many applications a knowledge of this low frequency behavior is sufficient, the field penetration through an aperture increases with an increase in frequency and the penetration of energy should be a maximum at the resonant frequency of the aperture (to see this one needs only to consider the quarter wave resonant slot antenna).

At low frequency, when the characteristic dimension of the aperture is much less than a wave length, the dipole moments of the magnetic source equivalent to the aperture field distribution may be used to obtain a very simple analytical expression for the penetration field (ref. 1). But the obtained expression is not valid for the region in proximity to the aperture. Unfortunately it is near the aperture that the penetration field is largest. Therefore, in studying the coupling of energy through an aperture a formulation for determining the near field behavior is needed. Moreover, the

---

1. Taylor, C. D., "Electromagnetic Pulse Penetration Through Small Apertures," AFWL Interaction Note 74, March 1971.

near field formulation could be used to determine the range of applicability of the simple analytical formulas based on the aforementioned dipole moment considerations.

Bethe (ref. 2) reported some time ago that the Kirchhoff approximation applied at low frequency provides an over estimate of the energy penetrating a small aperture in an infinite plate. It is well know that the Kirchhoff approximation yields accurate results in the high frequency regime where the operating wave length is much less than the characteristic dimension of the aperture (ref. 3). With a general formulation available for determining the penetration field of an aperture it may be possible to determine the frequency regime where using the Kirchhoff approximation is sufficient for determining the penetration field.

Because of the aforementioned reasons a general formulation unrestricted in frequency is needed for determining the electromagnetic field through apertures. A very elegant formulation developed by Flammer (ref. 4) is available. However, the solution is expressed in terms of the not-too-well tabulated oblate spheroidal wave functions. But the integral equation formulation developed by Andreason (ref. 5) for treating scattering from bodies of revolution may be adapted also to determine the electromagnetic

---

2. Bethe, H. A., "Theory of Diffraction by Small Holes," Phy. Rev., Vol. 66, pp. 163-182, October 1944.

3. Jones, D. S., The Theory of Electromagnetism. Pergamon Press, New York, 1964, pp. 626-640.

4. Flammer, C., "The Vector Wave Function Solution of the Diffraction of Electromagnetic Waves by Circular Disks and Apertures. II. The Diffraction Problems," J. Appl Phys., Vol. 24, No. 9, pp. 1224-1231, September 1953.

5. Andreason, M. G., "Scattering from Bodies of Revolution," IEEE Trans. Ant. and Prop., Vol. AP-13, pp. 303-310, March 1965.

field penetration through a circular aperture in a plate. Because it is believed to be more convenient the integral equation formulation is used by the authors in developing a theoretical-numerical formulation of aperture penetration.

The solution technique for determining the electromagnetic field diffracted by an aperture begins with the solving of the complimentary disk problem and applying Babinet's principle (ref. 4). Since a disk is a limiting form of a body of revolution, the integral equation developed by Andreason (ref. 5) for bodies of revolution may be used to obtain the induced current distribution on the disk. The field scattered from the disk is determined directly from the induced current. Appropriately transforming this scattered field using Babinet's principle yields the diffraction field of a circular aperture in a conducting plate. In principle the resulting formulation is not limited in frequency and the near field as well as the far field may be obtained.

For pulse excitation it has been shown that the singularity expansion method is advantageous (ref. 6). Moreover the singularity expansion method may be readily applied to the presented integral equation formulation. A few preliminary results are presented.

Extensive comparisons are made with available measured data. Numerical convergence is examined. And comparisons with the aforementioned low frequency and high frequency approximations are discussed.

---

6. Baum, C. E., "On the Singularity Expansion Method for the Solution of Electromagnetic Interaction Problems," AFWL Interaction Note 88, December 1971.

SECTION II

ANALYSIS

1. INTEGRAL EQUATIONS

Applying the integral equation given by Andreason (ref. 5) to determine the surface current density, $\vec{J}_s$, induced on a disk centered at the origin and in the z = 0 plane yields

$$\hat{t}_n' \cdot \vec{E}^i(\vec{r}') = \frac{j\omega\mu}{4\pi k^2} \hat{t}_n' \cdot [k^2 \int_S \vec{J}_s(\vec{r}) G(\vec{r}|\vec{r}') ds + \text{grad}' \int \text{div } \vec{J}_s(\vec{r}) G(\vec{r}|\vec{r}') ds] \quad (1)$$

where $\hat{t}_1' = \hat{r}'$ and $\hat{t}_2' = \hat{\phi}'$ with

$$G(\vec{r}|\vec{r}') = \frac{e^{-jk|\vec{r} - \vec{r}'|}}{|\vec{r} - \vec{r}'|}$$

Assuming an incident plane wave field and expanding in a TM mode expansion yields

$$\vec{E}_1^i(\vec{r}) = \sum_{m=0}^{\infty} [E^e_{1,m}(r) \cos m\phi \, \hat{r} + E^o_{2,m}(r) \sin m\phi \, \hat{\phi}] \cdot e^{-jkz \cos \theta_i} \quad (2)$$

where θ_i is the angle between the incident $\vec{k}$ vector and the negative z-axis. In a similar fashion the TE mode expansion for the incident plane wave is

$$\vec{E}_1^i(\vec{r}) = \sum_{m=0}^{\infty} [E^o_{1,m}(r) \sin m\phi \, \hat{r} - E^e_{2,m}(r) \cos m\phi \, \hat{\phi}] \cdot e^{-jkz \cos \theta_i} \quad (3)$$

For the TM mode the expansion for the induced current density distribution on the disk is

$$\vec{J}_s(\vec{r}) = \sum_{m=0}^{\infty} [K^e_{1,m}(r) \cos m\phi \, \hat{r} + K^o_{2,m}(r) \sin m\phi \, \hat{\phi}] \tag{4}$$

and, correspondingly, for the TE mode

$$\vec{J}_s(\vec{r}) = \sum_{m=0}^{\infty} [K^o_{1,m}(r) \sin m\phi \, \hat{r} - K^e_{2,m}(r) \cos m\phi \, \hat{\phi}] \tag{5}$$

Using Equations (2) and (4) in (1) yields the coupled equations for $K^e_{1,m}$ and $K^o_{2,m}$ where

$$G_m(r|r') = \int_0^{\pi} \frac{e^{-jkR}}{R} \cos m\phi \, d\phi \tag{6}$$

and

$$R = [(r - r')^2 + 2rr'(1 - \cos\phi)]^{1/2}$$

$$E^e_{1,m}(r') = j \frac{\zeta k}{4\pi} \left[\int_o^a [G_{m-1}(r|r') + G_{m+1}(r|r')] K^e_{1,m}(r) r dr \right.$$

$$+ \frac{2}{k^2} \frac{d}{dr'} \int_o^a G_m(r|r')(r \frac{d}{dr} + 1) K^e_{1,m}(r) dr$$

$$- \int_o^a [G_{m-1}(r|r') - G_{m+1}(r|r')] K^o_{2,m}(r) r dr$$

$$\left. + \frac{2m}{k^2} \frac{d}{dr'} \int_o^a G_m(r|r') K^o_{2,m}(r) dr \right] \tag{7}$$

and

$$E^o_{2,m}(r') = j\frac{\zeta k}{4\pi}\left[-\int_o^a [G_{m-1}(r|r') - G_{m+1}(r|r')]K^e_{1,m}(r)rdr\right.$$

$$-\frac{2m}{k^2r'}\int_o^a G_m(r|r')(r\frac{d}{dr}+1)K^e_{1,m}(r)dr$$

$$+\int_o^a [G_{m-1}(r|r') + G_{m+1}(r|r')]K^o_{2,m}(r)rdr$$

$$\left.-\frac{2m^2}{k^2r'}\int_o^a G_m(r|r')K^o_{2,m}(r)dr\right] \qquad (8)$$

Using Equations (3) and (5) in (1) yields similar coupled equations for $K^o_{1,m}$ and $K^e_{2,m}$ which may be obtained from Equations (7) and (8) making the replacements

$$K^e_{1,m} \rightarrow K^o_{1,m}$$

$$K^o_{2,m} \rightarrow K^e_{2,m}$$

$$E^e_{1,m} \rightarrow E^o_{1,m}$$

$$E^o_{2,m} \rightarrow E_{2,m}$$

2. NUMERICAL SOLUTION BY THE METHOD OF MOMENTS

To obtain a numerical solution for Equations (7) and (8) it is necessary to investigate the apparent singularities that occur in the various integral and derivative terms. It is convenient to rewrite Equation (6) as

$$G_m(r|r') = 2\int_0^{\pi/2} \frac{e^{-jkR}\cos 2m\psi - 1}{R}\, d\psi$$

$$+\frac{2}{r+r'}K\left[1-\left(\frac{r-r'}{r+r'}\right)^2\right] \qquad (9)$$

where

$$K\left[1-\left(\frac{r-r'}{r+r'}\right)^2\right] = \int_0^{\pi/2} \frac{d\Psi}{\sqrt{1-\left[1-\left(\frac{r-r'}{r+r'}\right)^2\right]\sin^2\Psi}} \qquad (10)$$

or a complete elliptic integral of the first kind. Using L'Hospital's rule it can be shown that the first integral in Equation (9) is indeed a proper integral whose value can be obtained using ordinary numerical methods. In the elliptic integral there is an apparent singularity at $r=r'$ and K cannot be evaluated in its present form.

The numerical solution to Equations (7) and (8) will be obtained by the method of moments (ref. 7) using a piece-wise constant representation and point matching. For example

$$K^e_{1,m}(r) = \sum_{n=2}^{N-1} \alpha_n^m [H(r-r_n) - H(r-r_{n+1})]$$

$$+ \alpha_1^m H(r_2-r) + \alpha_N^m H(r-r_N) \qquad (11)$$

where

$$H(b) = 1 \text{ if } b > 0$$

$$H(b) = 0 \text{ if } b < 0$$

That is, the disk is divided into N zones with current zone bounds at

$$r = r_J = (J-1)\Delta \qquad \Delta = a/N \qquad J = 1,\cdots,N+1$$

and within a given zone the current has a constant value. In a similar manner $K^o_{2,m}$ is defined in terms of a set of expansion coefficients $\beta_1^m, \cdots, \beta_N^m$. One often-used procedure in the method of moments is to use

7. R. F. Harrington, Field Computation by Moment Methods, The MacMillan Company, New York, 1968.

these expansion sets for $K^{e}_{1,m}$ and $K^{o}_{2,m}$ in Equations (7) and (8), require that the equations be satisfied at a particular set of r′ values (in this case $r' = r'_I = (I - 0.5)\Delta$), and solve the resulting matrix equation for the α's and β's. Performing these operations results in the matrix equation

$$\sum_{J=1}^{2N} S(m,I,J)F(m,J) = \Gamma(m,I) \qquad (12)$$

The elements in Equation (12) are

$$F(m,J) = \alpha^{m}_{J} \qquad J = 1, \cdots, N$$

$$= \beta^{m}_{J-N} \qquad J = N + 1, \cdots, 2N$$

$$\Gamma(m,I) = -j \frac{4\pi}{\zeta k} E^{e}_{1,m}(r'_I) \qquad I = N, \cdots, N - 1$$

$$= -j \frac{4\pi}{\zeta k} E^{o}_{2,m}(r'_I) \qquad I = N, \cdots, 2N - 2$$

$$= 0 \qquad I = 2N - 1, 2N$$

$$S(m,I,1) = +\Delta F1(m - 1,I,1) - F2(m - 1,I,1) + \Delta F1(m + 1,I,1)$$

$$-F2(m + 1,I,1) - \frac{2}{k^2} [r_2 \, GMP(I,2) - F1P(m,I,1)]$$

$$I = 1, \cdots, N - 1$$

$$S(m,I,J) = +\Delta F1(m - 1,I,J) - F2(m - 1,I,J) + \Delta F1(m + 1,I,J)$$

$$- F2(m + 1,I,J) + r_J[F1(m - 1,I,J) + F1(m + 1,I,J)]$$

$$+\frac{2}{k^2} [r_J \, GMP(I,J) - r_{J+1} GMP(I,J+1) + F1P(m,I,J)]$$

$$J = 2, \cdots, N - 1$$

$$I = 1, \cdots, N - 1$$

$$S(m,I,N) = +\Delta F1(m-1,I,N) - F2(m-1,I,N) + \Delta F1(m+1,I,N)$$

$$- F2(m+1,I,N) + r_N[F1(m-1,I,N) + F1(m+1,I,N)]$$

$$+ \frac{2}{k^2}[r_N\, GMP(I,N) + FIP(m,I,N)]$$

$$I = 1, \cdots, N-1$$

$$S(m,I,J+N) = -\Delta F1(m-1,I,J) + F2(m-1,I,J) + \Delta F1(m+1,I,J)$$

$$- F2(m+1,I,J) - r_J[F1(m-1,I,J) - F1(m+1,I,J)]$$

$$- \frac{2m}{k^2} F1P(m,I,J)$$

$$I = 1, \cdots, N-1$$

$$J = 1, \cdots, N$$

$$S(m,I+N-1,1) = -\Delta F1(m-1,I,1) + F2(m-1,I,1) + \Delta F1(m+1,I,1)$$

$$- F2(m+1,I,1) + \frac{2m}{k^2 r_I'}[r_2 GM(I,2) - F1(m,I,1)]$$

$$I = 1, \cdots, N-1$$

$$S(m,I+N-1,J) = -\Delta F1(m-1,I,J) + F2(m-1,I,J) + \Delta F1(m+1,I,J)$$

$$-F2(m+1,I,J) - r_J[F1(m-1,I,J) - F1(m+1,I,J)]$$

$$- \frac{2m}{k^2 r_I'}[r_J GM(I,J) - r_{J+1} GM(I,J+1) + F1(m,I,J)]$$

$$I = 1, \cdots, N-1$$

$$J = 2, \cdots, N-1$$

$$S(m,I+N-1,N) = -\Delta F1(m-1,I,N) + F2(m-1,I,N) + \Delta F1(m+1,I,N)$$

$$- F2(m+1,I,N) - r_N[F1(m-1,I,N) - F1(m+1,I,N)]$$

$$- \frac{2m}{k^2 r_I'}[r_N GM(I,N) + F1(m,I,N)]$$

$$I = 1, \cdots, N-1$$

$$S(m,I+N-1,J+N) = \Delta F1(m-1,I,J) - F2(m-1,I,J) + \Delta F1(m+1,I,J)$$

$$- F2(m+1,I,J) + r_J[F1(m-1,I,J) + F1(m+1,I,J)]$$

$$- \frac{2m^2}{k^2 r_I'} F1(m,I,J)$$

$$I = 1, \cdots, N-1$$

$$J = 1, \cdots, N$$

This completes the definition of all elements in the matrix equation apart from the last two rows of the S matrix. The F matrix in Equation (12) has 2N unknowns, but only 2N - 2 matchpoints have been specified leading to 2N - 2 equations. Rather than match in the last zone which could lead to difficulties due to the edge effects, the edge conditions of the components of the current density are used to obtain the remaining two equations.*

The edge condition for the radial component of current requires (ref. 8)

$$K^e_{1,m}(r) \simeq A(a^2 - r^2)^{1/2}$$

and for the azimuthal component of current requires

$$K^o_{2,m}(r) \simeq B(a^2 - r^2)^{-1/2}$$

for $(r-a)/a \ll 1$. The piece-wise constant current in the last two zones is required to satisfy the foregoing. Considering the radial component of current yields

---

*Using the novel approach of requiring the current expansion to satisfy the edge conditions explicitly, resulted in a considerable improvement in the numerical convergence.

8. Meixner, V. J. and Andrejewski, W, "Strenge Theorie der Beugung ebener elektromagnetischer Wellen an der Vollkommen leitenden Kreisscheibe und an der kreisformigen Offnung im vollkommen leitenden ebenen Schirm," Annalen der Physik, Band 7, pp. 157-168, 1950.

$$\alpha_N(a\Delta - .25\Delta^2)^{-1/2} - \alpha_{N-1}(3a\Delta - 2.25\Delta^2)^{-1/2} = 0 \qquad (13)$$

and a similar equation for β_N and β_{N-1} is obtained from the edge condition of the azimuthal component of current. Thus

$$S(m,2N-1,N) = (a\Delta - .25\Delta^2)^{-1/2}$$

$$S(m,2N-1,N-1) = -(3a\Delta - 2.25\Delta^2)^{-1/2}$$

$$S(m,2N,2N) = (a\Delta - .25\Delta^2)^{-1/2}$$

$$S(m,2N,2N-1) = -(3a\Delta - 2.25\Delta^2)^{-1/2}$$

and hence the last two rows of Γ are zero. The terms in S are defined by

$$F1(m,I,J) = \int_0^\Delta g_m(u + r_J|r_I)du + 2\int_0^\Delta \frac{1}{u + r_J + r_I'} K\left[1 - \left(\frac{u + r_J - r_I'}{u + r_J + r_I'}\right)^2\right] du \qquad (14)$$

$$F1P(m,I,J) = \frac{d}{dr_I'} F1(m,I,J) \qquad (15)$$

$$F2(m,I,J) = \Delta F1(m,I,J) - \int_0^\Delta g_m(u + r_J|r_I')u\,du - 2\int_0^\Delta \frac{u}{u + r_J + r_I'} K\left[1 - \left(\frac{u + r_J - r_I'}{u + r_J + r_I'}\right)^2\right] du \qquad (16)$$

$$GM(I,J) = G_m(r_J|r_I') \qquad (17)$$

$$GMP(I,J) = \frac{d}{dr_I'} GM(I,J) \qquad (18)$$

$$g_m(r|r') = 2\int_0^{\pi/2} \frac{e^{-jkR}\cos 2m\Psi - 1}{R}\, d\Psi \tag{19}$$

$$R = [(r - r')^2 + 4rr' \sin^2\Psi]^{1/2} \tag{20}$$

This completes the definition of all terms in Equation (12) for the TM case. In an analogous fashion an equation for the TE case can be constructed.

To illustrate the numerical techniques employed consider the expression F1(m,I,J). The first term can be evaluated by ordinary numerical integration since it contains no apparent singularities. The second term

$$F12(m,I,J) = 2\int_0^{\Delta} \frac{1}{u + r_J + r_I'} K\left[1 - \left(\frac{u + r_J - r_I'}{u + r_J + r_I'}\right)^2\right] du \tag{21}$$

has an apparent singularity at $u = 0.5\Delta$ when $I = J$. K is approximated by (ref. 9)

$$K(m) = a_0 + a_1 m_1 + a_2 m_1^2 + a_3 m_1^3 + a_4 m_1^4 + [b_0 + b_1 m_1 + b_2 m_1^2 + b_3 m_1^3 + b_4 m_1^4] \ln(1/m_1) \tag{22}$$

where

$$a_0 = 1.386\ 294\ 4$$

$$a_1 = 0.096\ 663\ 443$$

$$a_2 = 0.035\ 900\ 924$$

$$a_3 = 0.037\ 425\ 637$$

$$a_4 = 0.014\ 511\ 962$$

$$b_0 = 0.5$$

$$b_1 = 0.124\ 985\ 94$$

---

9. Abramowitz, M. and Stegun, I. A., editors, Handbook of Mathematical Functions. Dover Publications, Inc., New York, 1965, p. 591.

$$b_2 = 0.068\ 802\ 486$$

$$b_3 = 0.033\ 283\ 553$$

$$b_4 = 0.004\ 417\ 870$$

$$m + m_1 = 1$$

Rewriting Equation (21) gives

$$F12(m,I,J) = 2\int_{o}^{.5\Delta\ \varepsilon} I(u)du + \lim_{h_1 \to .5\Delta-} 2\int_{.50\Delta-\varepsilon}^{h_1} I(u)\ du$$

$$+ \lim_{h_2 \to .5\Delta+} 2\int_{h_2}^{.5\Delta+\varepsilon} I(u)du + 2\int_{.5\Delta+\varepsilon}^{\Delta} I(U)\ du \qquad (23)$$

If, in the second and third integrals of Equation (23), only the a_o and b_o terms in K are retained, the integrations can be analytically performed. Evaluation of these expressions shows that F1(m,I,J) exists in the Cauchy Principle Value sense (ref. 10). The calculations are straightforward but cumbersome and will not be included.

The evaluation of the F1P(m,I,J) terms is accomplished by taking the partial derivative of all terms in F1, except I_2 and I_3 of Equation (23), and numerically those integrals. For I_2 and I_3, the partial derivative of the analytic expressions for the Cauchy values is taken. The apparent singularity in F2(m,I,J) when I = J is treated exactly as described for F1(m,I,J). All other elements of S can be evaluated by standard numerical methods.

---

10. Edwards, J., Treatise on Integral Calculus, Vol. I, Chelsea Publishing co., New York, 1954, pp. 340-349

Since the S elements require considerable computing time only the case of normal incidence on the disk was investigated in detail. For this problem only the m = 1 mode need be considered. The incident field may be expanded as (ref. 11)

$$E^e_{1,m}(r) = -\cos\theta_p \cos\theta_i \, \varepsilon_m j^{m+1} J'_m(kr \sin\theta_i) E_o$$

$$E^o_{2,m}(r) = \cos\theta_p \cos\theta_i \, \varepsilon_m j^{m+1} \, m \frac{J_m(kr \sin\theta_i)}{kr \sin\theta_i} \tag{24}$$

for the TM case with r,ϕ,z the usual cylindrical coordinates and the angles of incidence and polarization defined as in Figure 1.

For the TE mode

$$E^o_{1,m}(r) = -\sin\theta_p \, \varepsilon_m j^{m+1} \, m \frac{J_m(kr \sin\theta_i)}{kr \sin\theta_i} \, E_o$$

$$E^e_{2,m}(r) = \sin\theta_p \, \varepsilon_m j^{m+1} J'_m(kr \sin\theta_i) \, E_o \tag{25}$$

where ε_m is the Neumann number defined

$$\varepsilon_m = \begin{cases} 2 & m = 0 \\ 1 & \text{otherwise} \end{cases} \tag{26}$$

and J_m the Bessel functions. Recursion relations among the Bessel functions can be used to show that for $\theta_i = 0$ or π,

$$E^e_{1,m}(r) = \cos\theta_p \, E_o \, \delta_{m,1} \cos\theta_i$$

$$E^o_{2,m}(r) = -\cos\theta_p \, E_o \, \delta_{m,1} \cos\theta_i$$

$$E^o_{1,m}(r) = \sin\theta_p \, E_o \, \delta_{m,1} \, |\cos\theta_i| \tag{27}$$

$$E^e_{2,m}(r) = -\sin\theta_p \, E_o \, \delta_{m,1} \, |\cos\theta_i|$$

---

11. Stratton, J. A., Electromagnetic Theory. McGraw-Hill Book Company, New York, 1941, pp. 371-372.

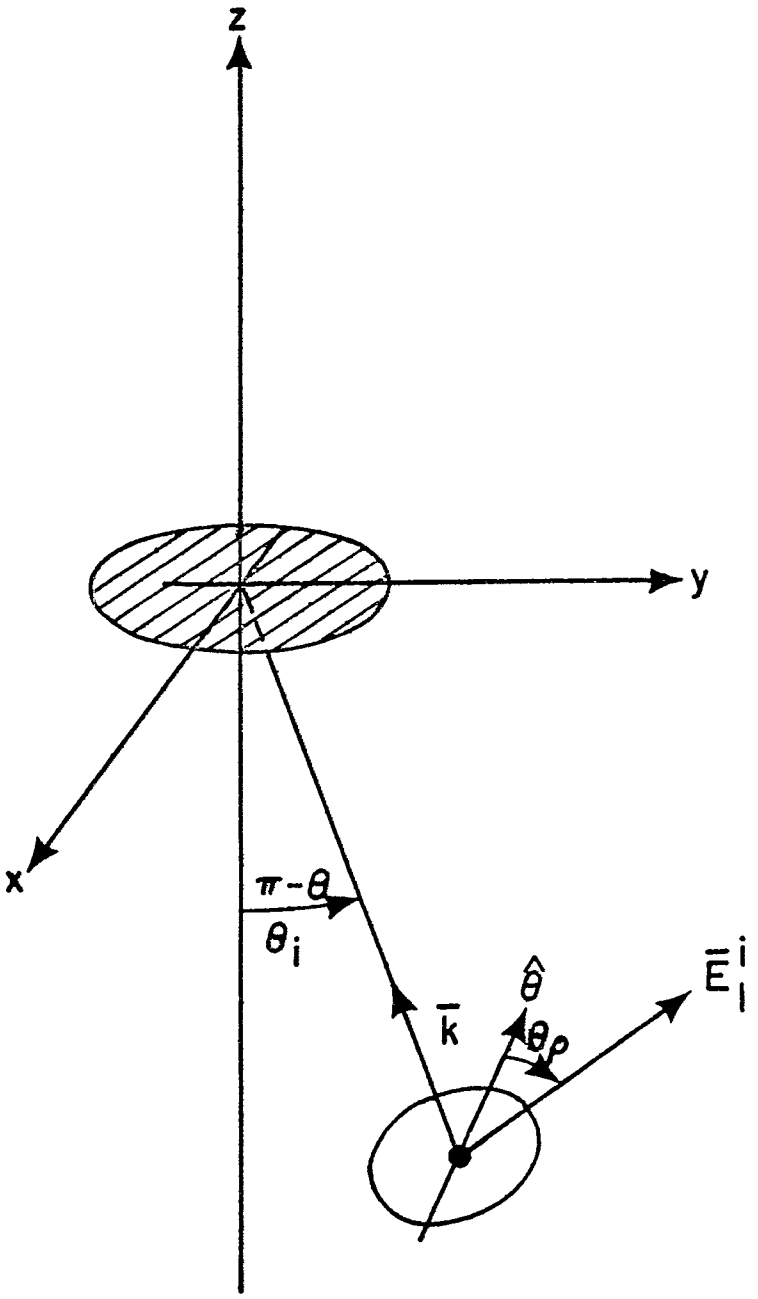

Figure 1. Circular Disk with the Polarization of the Incident Field

where $\delta_{m,1}$ is the Kronecker δ.

3. SCATTERED FIELD COMPUTATION

Maxwell's equations lead to the following for the scattered fields once the induced surface current density is known:

$$\vec{E}_1^s(r') = -j \frac{\zeta}{4\pi k} \left[\nabla' \int_s \nabla \cdot \vec{J}_s(\vec{r})\, G(\vec{r}|\vec{r}')\, ds + k^2 \int_s \vec{J}_s(\vec{r})\, G(\vec{r}|\vec{r}')\, ds \right] \tag{28}$$

$$\vec{H}_1^s(\vec{r}') = \frac{1}{4\pi} \int_s \vec{J}_s(\vec{r}) \times \nabla\, G(\vec{r}|\vec{r}')\, ds \tag{29}$$

with

$$G = \frac{e^{-jkR}}{R}$$

$$R = \sqrt{r^2 + r'^2 - 2rr' \sin\theta' \cos(\phi - \phi')}$$

These expressions can be expanded in terms of cartesian components and evaluated for the various field points. There are two difficulties encountered with Equations (28) and (29): each integrand becomes unbounded as $r \to a$ since $J_{s\phi} \to \infty$ at this point, and the equations are not valid for points in or on the source. For convenience the field points are limited to the axis of the disk (along z). For a normally incident field polarized in the x direction on a disk in the $z = 0$ plane, only E_{1x}^s and H_{1y}^s need be calculated. The result of the analytical integration near $r = a$ leads to

$$E^{s}_{1x} = -\frac{j\zeta}{4\pi}\int_{o}^{a-\delta}\int_{o}^{2\pi}\Bigg[-k^2[J_{sr}z\sin\theta'\cos(\phi-\phi') - J_{sr}\,r + J_{s\phi}\,z$$

$$\sin\theta'\cos(\phi+\pi/2-\phi')]\cdot[z\sin\theta'\cos\phi' - r\cos\phi]/R^2$$

$$+\frac{1}{R}\left(jk+\frac{1}{R}\right)[3\left[J_{sr}z\sin\theta'\cos(\phi-\phi') - J_{s}\,r + J_{s\phi}\,z\sin\theta'\cdot\right.$$

$$\left.\cos\left(\phi+\frac{\pi}{2}-\phi'\right)\right]\cdot\left[z\sin\theta'\cos\phi' - r\cos\phi\right]/R^2$$

$$\left.-J_{sr}\cos\phi + J_{s\phi}\sin\phi] + k^2 J_{sr}\cos\phi - k^2 J_{s\phi}\sin\phi\;\; G(r|z)\right]\,r\,dr\,d\phi$$

$$-\frac{j\zeta}{4\pi k}\frac{1}{R}\left(jk+\frac{1}{R}\right)G(a|z)\,a\cdot\Big[K^{e}_{1,1}(r_N')[a^2-(a-\tfrac{\Delta}{2})^2]^{-1/2}$$

$$\left[\frac{a^2\pi}{4} - \frac{(a-\delta)}{2}(a^2-(a-\delta)^2)^{1/2} - \frac{a^2}{2}\arcsin\frac{(a-\delta)}{a}\right]\pi$$

$$+K^{o}_{1,1}(r_N')\,[a^2-(a-\tfrac{\Delta}{2})^2]^{1/2}\left[\frac{\pi}{2} - \arcsin\left(\frac{a-\delta}{a}\right)\pi\right]$$

$$-\frac{j\zeta}{4\pi k}[G(a|z)a]\Big[k^2K^{e}_{1,1}(r_N')\,[a^2-(a-\tfrac{\Delta}{2})^2]^{-1/2}\left[\frac{a^2\pi}{4} - \left(\frac{a-\delta}{2}\right)\cdot\right.$$

$$(a^2-(a-\delta)^2)^{1/2} - \frac{a^2}{2}\arcsin\left(\frac{a-\delta}{a}\right)]\pi - k^2K^{o}_{1,1}(r_N')[a^2-(a-\tfrac{\Delta}{2})^2]^{1/2}$$

$$\left.\left[\frac{\pi}{2} - \arcsin\left(\frac{a-\delta}{a}\right)\right]\pi\Big] \qquad (30)$$

where

$$\theta' = 0$$

$$\phi' = 0$$

$$\delta = a/N$$

$$R = [r^2+z^2]^{1/2}$$

$$r_I' = \Delta(I-0.5) \qquad I = 1, \cdots, N$$

In a similar fashion H^s_{1y} can be evaluated. The tabulated values of the current densities and Simpson's rule integration lead to the scattered fields from the disk. Babinet's principle is then used to calculate the scattered fields for the equivalent aperture

4. SINGULARITY EXPANSION METHOD

To apply the singularity expansion method it is necessary to perform a pole search on the S matrix of (12), i.e. S is a function of the complex frequency, $s = \sigma + j\omega$, and the roots of the determinant of S are found by a numerical search routine. Accordingly the current density may be represented (ref. 12).

$$[\bar{J}_s(s)] = \sum_\alpha \frac{[\bar{\bar{R}}_\alpha][\bar{E}(s_\alpha)]}{s - s_\alpha}$$

where

$[\bar{J}_s(s)]$	is a column vector containing the radial and circumferential components of the mode current density
$[\bar{\bar{R}}_\alpha]$	is the residue matrix
$[\bar{E}(s_\alpha)]$	the excitation field vector
s_α	the poles of the system matrix

The foregoing does not show explicitly the mode contributions. Actually each modal contribution should be expanded as shown above and the sum of the modal contributions would represent the total surface current density.

The scattered fields in the time domain can be obtained using the singularity expansion method from equation (30) by introducing s, the complex frequency, and replacing the current density by

---

12. Crow, T. T., Graves, B. D. and Taylor, C. D., "The Singularity Expansion Method as Applied to Perpendicular Crossed Cylinders in Free Space," AFWL Interaction Note 161, October 1973.

$$\frac{[\bar{J}_{sr}(s)]}{E_o \cos\phi} = \sum_{\alpha} \frac{[\bar{\bar{R}}_{r\alpha}][\bar{E}(s)]}{s - s_\alpha} \tag{31}$$

$$\frac{[\bar{J}_{s\phi}(s)]}{E_o \sin\phi} = \sum_{\alpha} \frac{[\bar{\bar{R}}_{\phi\alpha}][\bar{E}(s)]}{s - s_\alpha} \tag{32}$$

where $[\bar{\bar{R}}_{r\alpha}]$ and $[\bar{\bar{R}}_{\phi\alpha}]$ are rectangular arrays containing the first N rows of $[\bar{\bar{R}}_{\alpha}]$ and the last N rows of $[\bar{\bar{R}}_{\alpha}]$, respectively. In terms of mode and coupling vectors and coupling constants η_α, Equation (31) can be rewritten as

$$\frac{[\bar{J}_{sr}(s)]}{E_o \cos\phi} = \sum_{\alpha} \frac{\beta_\alpha [\bar{M}_{r\alpha}][\bar{C}_\alpha]^T [\bar{E}(s)]}{s - s_\alpha} \tag{33}$$

$$[\bar{J}_{sr}(s)] = \sum_{\alpha} \frac{\beta_\eta \eta_\alpha(s)[\bar{M}^{\phi}_{r\alpha}]}{s - s_\alpha} \tag{34}$$

$$\eta_\alpha(s) = [C_\alpha]^T [\bar{E}(s)] \tag{35}$$

and similar expressions for $[\bar{J}_{s\phi}(s)]$ can be obtained. These equations, (31) through (35), apply for normal incidence, m = 1. For other than normal incidence, each of Equations (31) through (34) must also include a summation over m.

For the normal incidence case, substitution of Equation (34) and its companion for $[\bar{J}_{s\phi}(s)]$ into Equation (30) leads to an expression for $E^s_{lx}(r',\phi',\theta',s)$ as a summation over poles. The time-domain response is found from

$$E^s_{lx}(r',\theta',\phi',t) = \frac{1}{2\pi j} \int_{\sigma c - j\infty}^{\sigma c + j\infty} E^s_{lx}(r',\phi',\theta',s) e^{st}\, ds \tag{36}$$

Performing the integration by the residue theorem and assuming a unit step electromagnetic pulse yields

$$E^{s}_{lx}(r', \phi', \theta', t) = \sum_{\alpha} \beta_{\alpha} \eta_{\alpha}(s_{\alpha}) \beta^{FE}_{\alpha x} e_{\alpha x}(r', \phi', \theta') e^{s_{\alpha} t} \tag{37}$$

$e_{\alpha x}$ is the electric field mode vector and the normalization factor $\beta^{FE}_{\alpha x}$ is defined such that the largest element of $e_{\alpha x}$ is real and has magnitude one. The explicit expression for $e_{\alpha x}$ is

$$\begin{aligned} e_{\alpha x}(r', \phi', \theta') = \frac{\zeta}{4\pi} \int_{o}^{a} \int_{o}^{2\pi} \Bigg[\Bigg(& [\bar{M}^{\phi}_{r\alpha}] \cdot r' \sin\theta' \cos(\phi - \phi') \\ & - [\bar{M}^{\phi}_{r\alpha}] r + [\bar{M}^{\phi}_{\phi\alpha}] r' \sin\theta' \cos(\phi + \pi/2 - \phi') \Bigg) \\ & \cdot [r' \sin\theta' \cos\phi' - r \cos\phi]/R^2 \\ & + \frac{1}{R} \left(1 + \frac{1}{R_{s\alpha}}\right) \Bigg[3 \Bigg(\frac{[\bar{M}^{\phi}_{r\alpha}]}{s_{\alpha}} r' \sin\theta' \cos(\phi - \phi') \\ & - \frac{[\bar{M}^{\phi}_{r\alpha}]}{s_{\alpha}} r + \frac{[\bar{M}^{\phi}_{\phi\alpha}]}{s_{\alpha}} r' \sin\theta' \cos\left(\phi + \frac{\pi}{2} - \phi'\right) \Bigg) \\ & \cdot \Big(r \sin\theta' \cos\phi' - r \cos\phi \Big)/R^2 \\ & - \frac{[\bar{M}^{\phi}_{r\alpha}]}{s_{\alpha}} \cos\phi + \frac{[\bar{M}^{s}_{\phi\alpha}]}{s_{\alpha}} \sin\phi \Bigg] - [\bar{M}^{\phi}_{r\alpha}] \cos\phi \\ & + [\bar{M}^{\phi}_{\phi\alpha}] \sin\phi \Bigg] \frac{e^{-s_{\alpha}R}}{R} \, r\,dr\,d\phi \end{aligned} \tag{38}$$

SECTION III

NUMERICAL RESULTS

1. CONVERGENCE OF THE SOLUTION

An important question occurring with the use of any numerical solution technique is the question of convergence. Here it is the question of how many current zones (N) must the disk be divided into to achieve the desired accuracy for the induced current calculation. A convenient means of making this determination is to use the low frequency analytical approximation for the surface current density induced on a circular disk illuminated by a plane wave propagating normal to the plane of the disk (ref. 13).

Considering a disk with a diameter small in terms of wavelength the current density is obtained numerically over a range of values for the number of current zones used. The data obtained are presented in Table 1 along with the low frequency approximation developed by Bouwkamp (ref. 13). From these data it is observed that numerical solution for the current density near the center of the disk convergences faster than the numerical solution for the current density near the edge. At N = 21 the numerical solution is within 10% of the low frequency for $r \lesssim a/2$. Probably the reason for the slower convergence of the solution for the current density near the edge is that the current density varies more rapidly with change in r in that region, particularly the azimuthal component of current. A graph of the induced surface current density is shown in figures 2 through 4.

---

13. Bouwkamp, C. J., "Diffraction Theory," Rep. Progr. Phys., 17, pp. 35-100, 1954.

TABLE 1. VARIATION OF CURRENT DENSITY VERSUS NUMBER OF ZONES ON A DISK OF DIAMETER 0.03183λ WITH NORMAL INCIDENCE

$\frac{r}{a}$	$J_r/\cos\phi \times kaE_o$	$J_\phi/\sin\phi \times kaE_o$
	N = 9	
.1667	j 0.005300	-j 0.005385
.5000	j 0.004806	-j 0.005731
.8333	j 0.003483	-j 0.008512
	N = 15	
.1667	j 0.004958	-j 0.005042
.5000	j 0.004478	-j 0.005377
.8333	j 0.003221	-j 0.007680
	N = 21	
.1667	j 0.004749	-j 0.004833
.5000	j 0.004276	-j 0.005167
.8333	j 0.003051	-j 0.007348
	N = 27	
.1667	j 0.004607	-j 0.004690
.5000	j 0.004138	-j 0.005026
.8333	j 0.002932	-j 0.007156
	N = 33	
.1667	j 0.004480	-j 0.004563
.5000	j 0.004014	-j 0.004902
.8333	j 0.002822	-j 0.007019
	N = 39	
.1667	j 0.004346	-j 0.004385
.5000	j 0.003854	-j 0.004744
.8333	j 0.002679	-j 0.006928
	Low Freq. Approximation	
.1667	j 0.004440	-j 0.004503
.5000	j 0.003900	-j 0.004550
.8333	j 0.002489	-j 0.005317

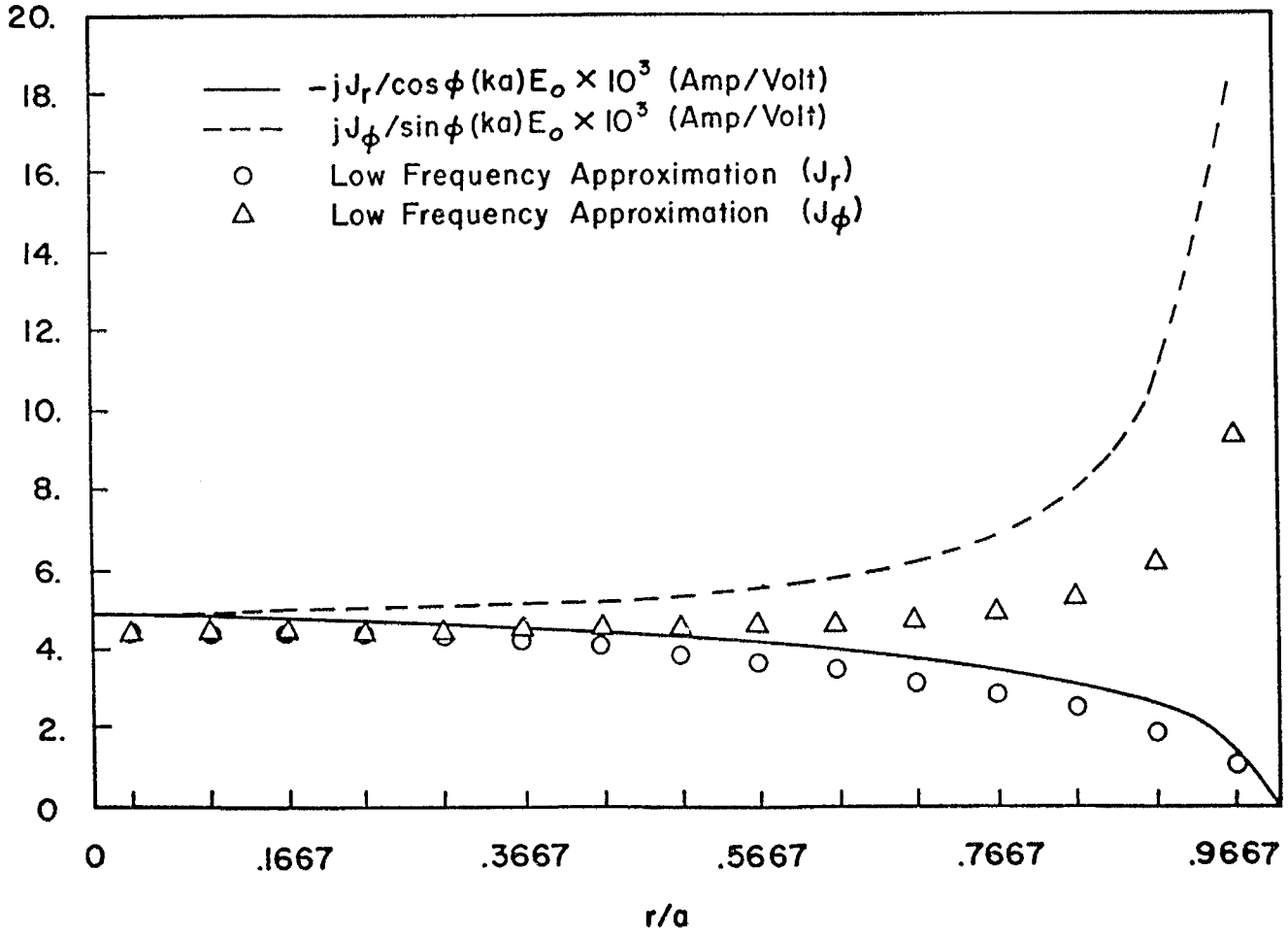

Figure 2. Distribution of Current Density on a Disk of Diameter .0636λ, for Normal Incidence with N = 15

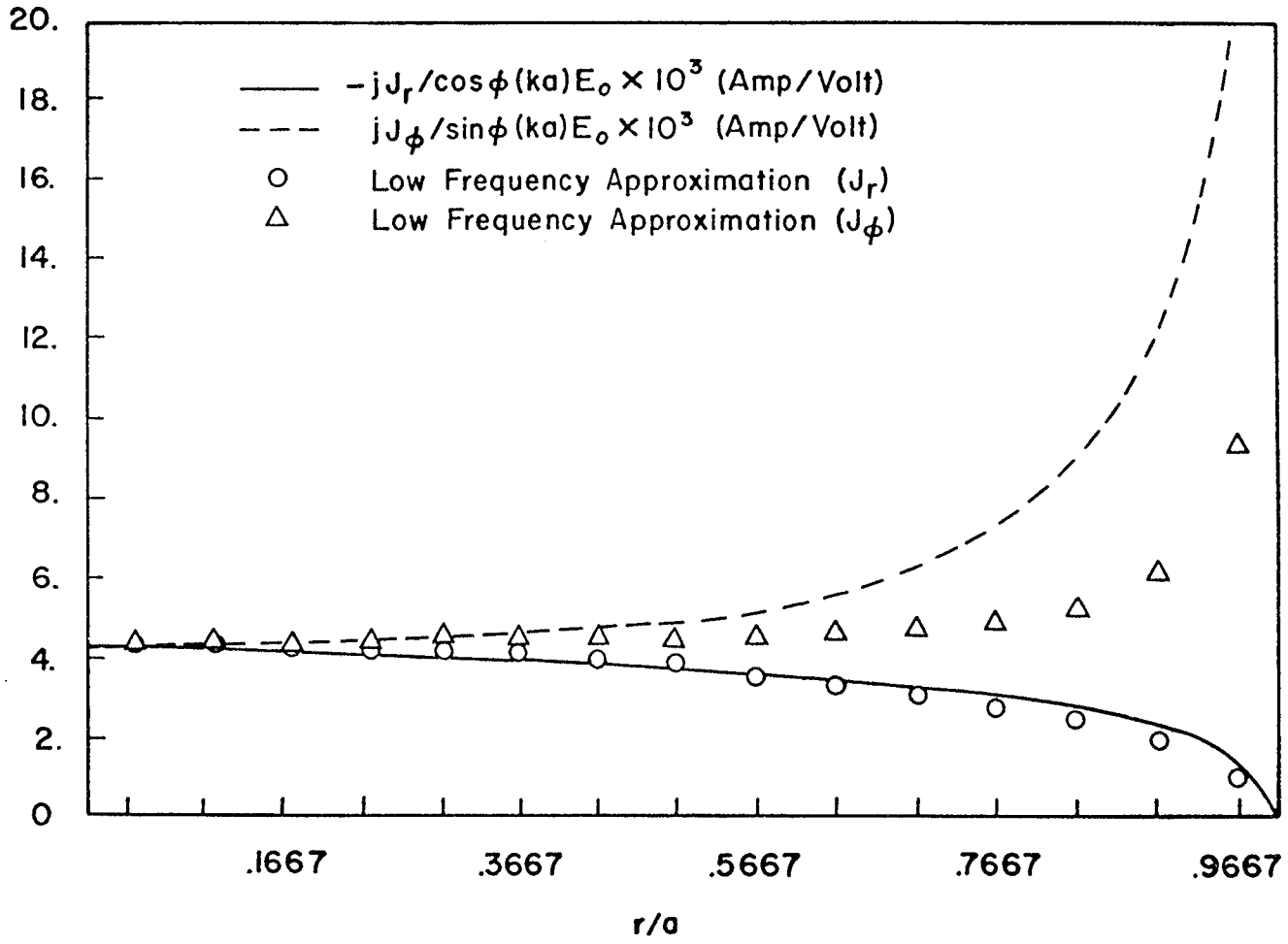

Figure 3. Distribution of Current Density on a Disk of Diameter .09549λ, for Normal Incidence with N = 15

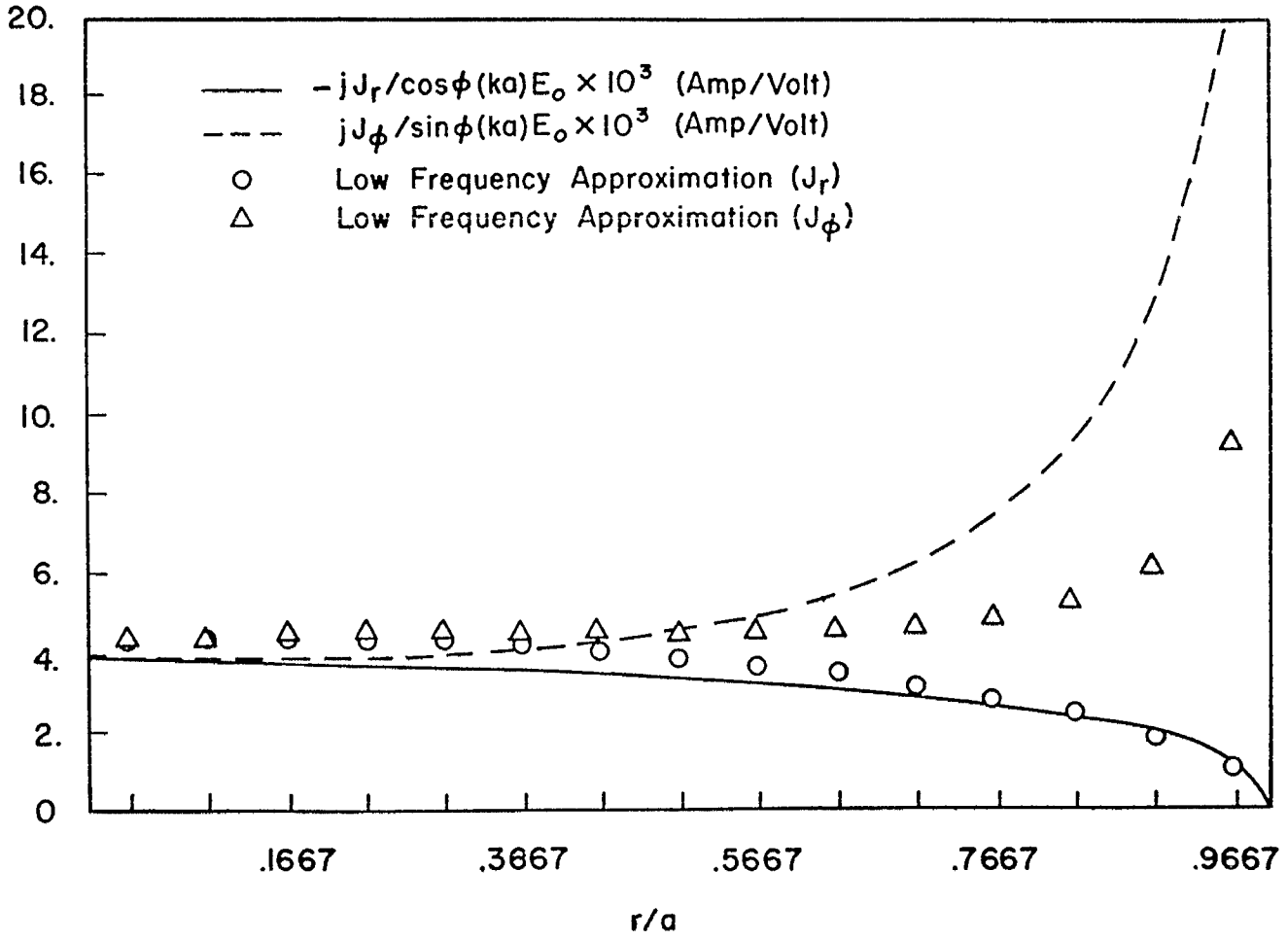

Figure 4. Distribution of Current Density on a Disk of Diameter .10345λ, for Normal Incidence with N = 15

As the frequency is increased the radial variation of the induced current density becomes more complex. This is seen in figures 5 through 7. In figures 5 and 6 current densities for $a = \lambda/4$ and $a = \lambda/2$, respectively, are shown. In both cases an apparently spurious oscillation occurs which decreased as N is increased. Hence this oscillation is probably related to the convergence of the numerical solution. Also shown on the foregoing graphs is the physical optics approximation (ref. 14), that should become more accurate at higher frequencies.

Apparently the numerical convergence is such that whenever $N > 20$, 10% accuracy is achieved for the current distribution near the center of the disk provided the frequency is not too high. Verification of the numerical results for higher frequencies is contained in the following section where comparisons are made with experimental data.

2. APERTURE FIELD DISTRIBUTION

To determine the accuracy of the integral equation results for high frequency illumination comparison with experimental data is made. The electromagnetic field distribution in a circular aperture has been measured by Buchsbaum et al. (ref. 15). Applying Babinet's principle and using the aforementioned results for the current induced on a circular disk yields the appropriate electric field component within an illuminated circular aperture to compare with the measured data of Buchsbaum, et al. In both

---

14. Harrington, R. F., Time Harmonic Electromagnetic Fields, McGraw-Hill Book Company, New York, 1961, pp. 127-128.

15. Buchsbaum, S. J., Milne, A. R., Hogg, D. C., Bekefi, G. and Woonton, G.A., "Microwave Diffraction by Apertures of Various Shapes," J. Appl. Phys., Vol. 26, pp. 706-715, June 1955.

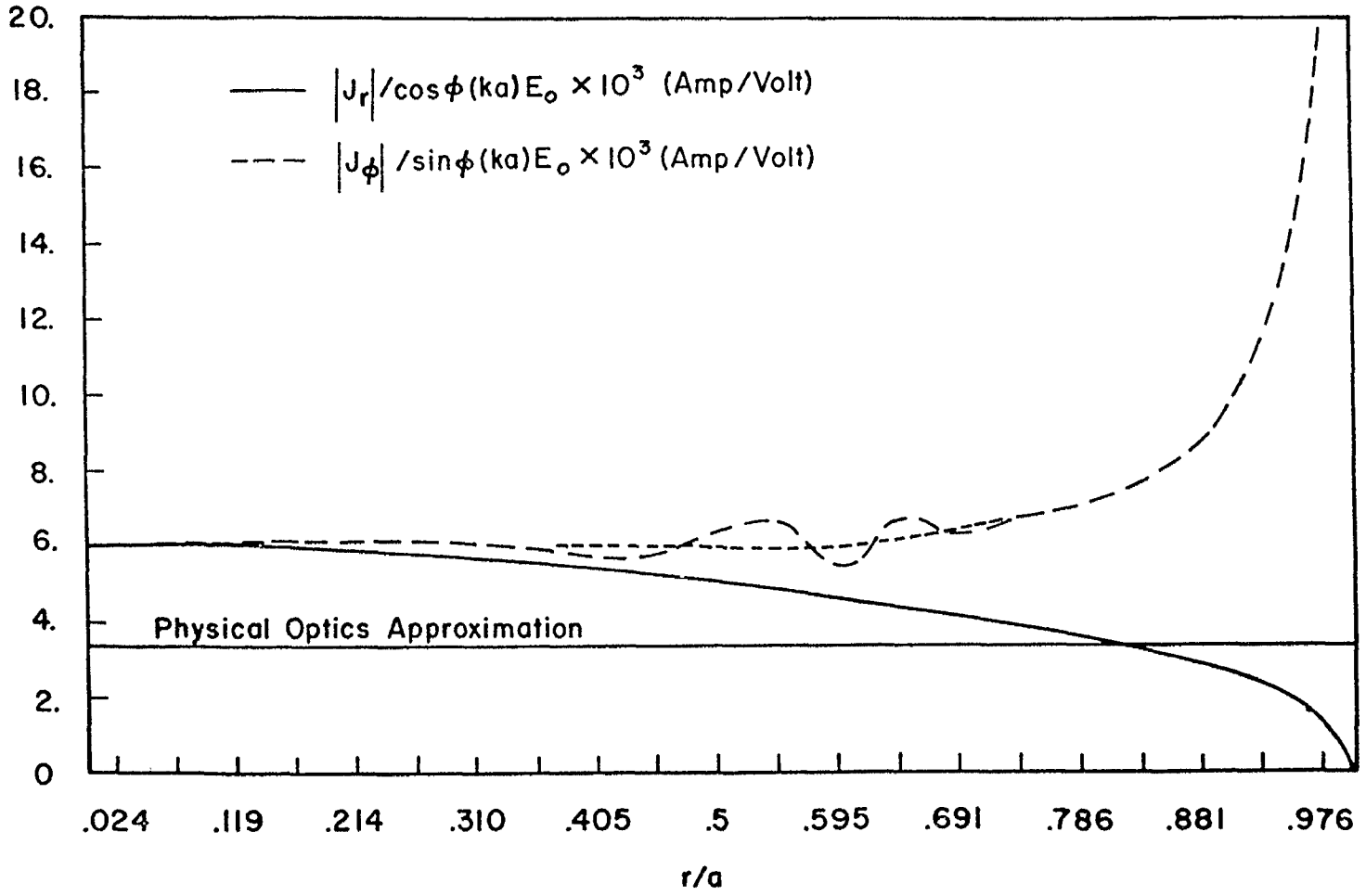

Figure 5. Distribution of Current Density on a Disk of Diameter .5λ, for Normal Incidence with N = 21

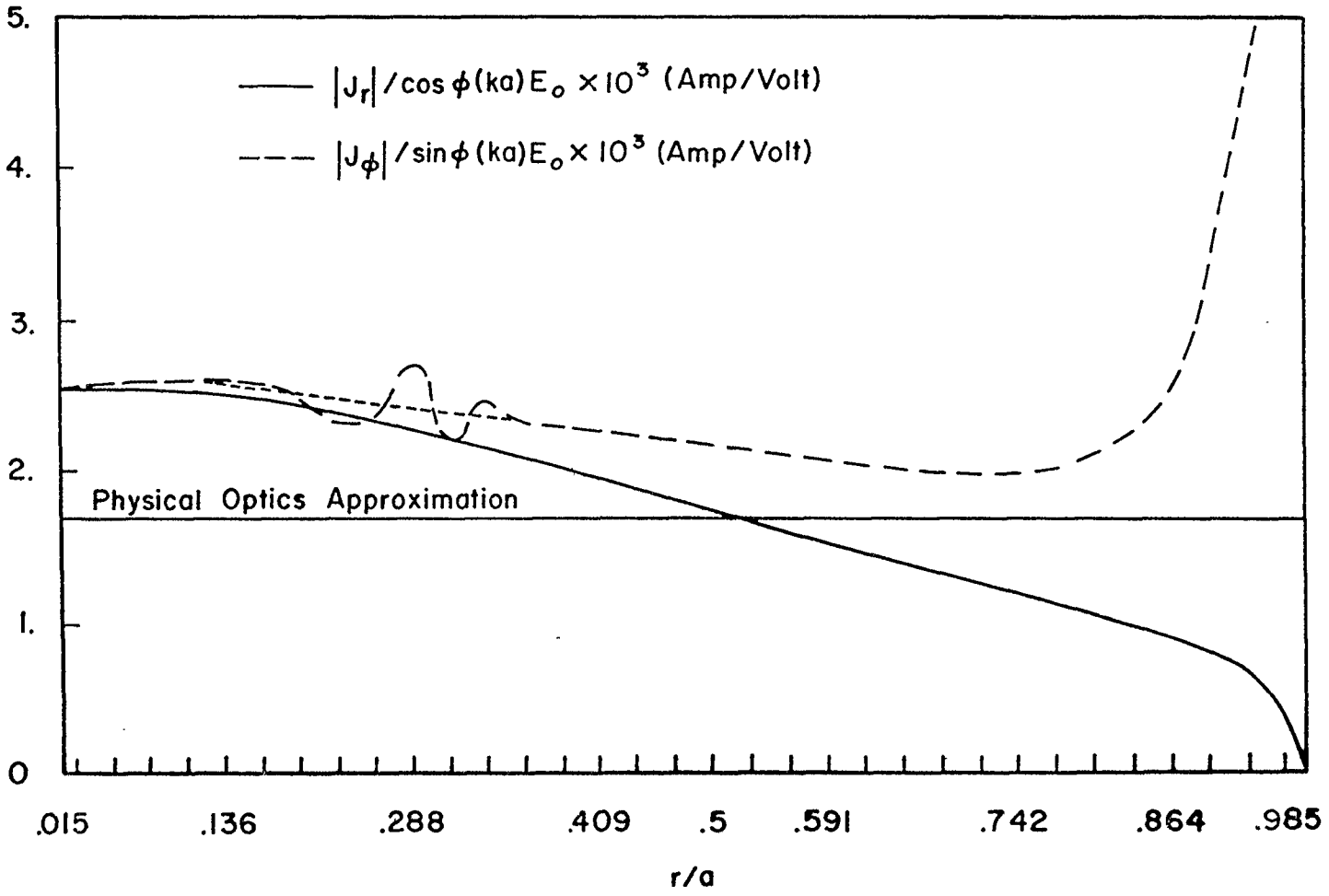

Figure 6. Distribution of Current Density on a Disk of Diameter 1.0λ for Normal Incidence with N = 33

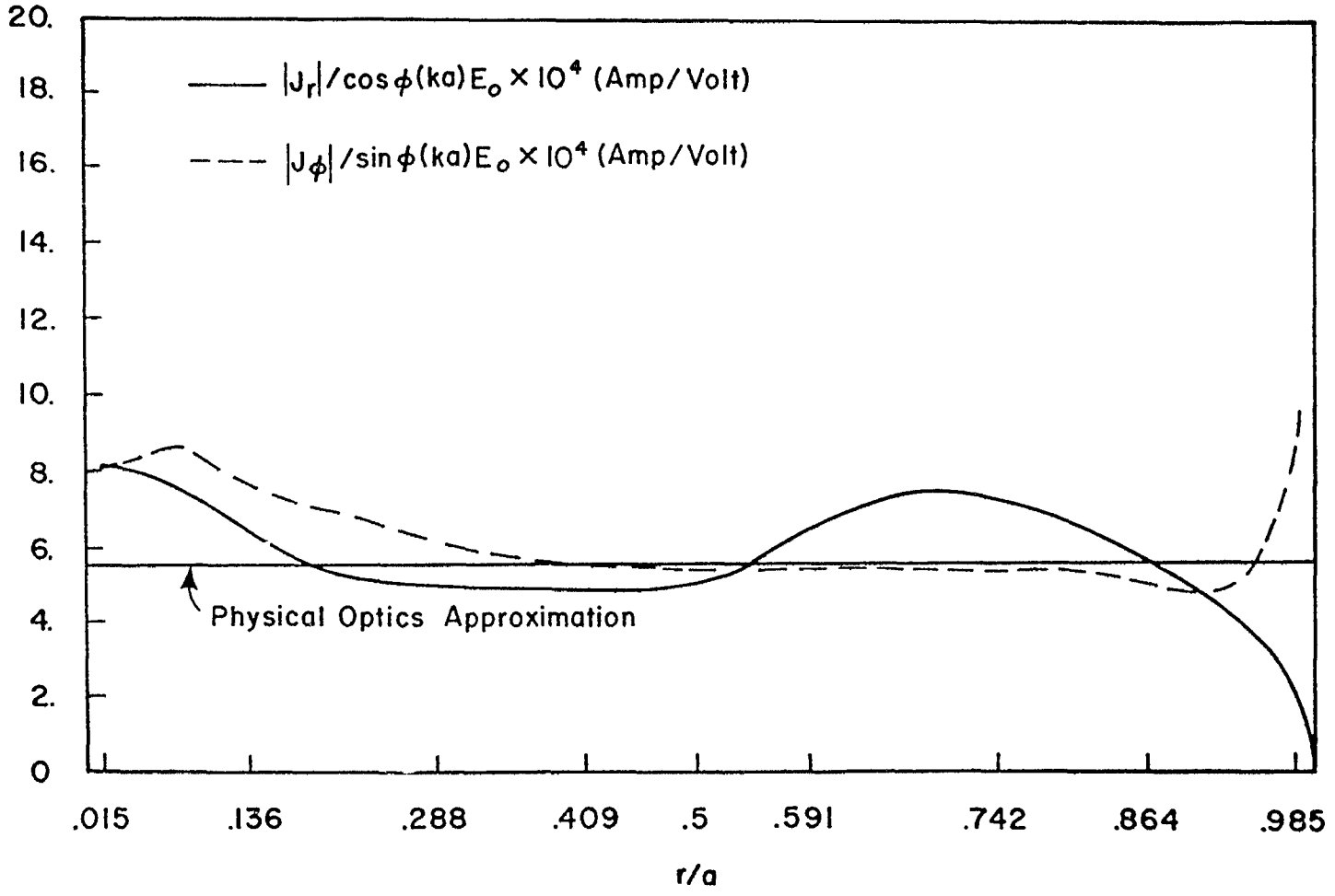

Figure 7. Distribution of Current Density on a Disk of Diameter 3λ for Normal Incidence with N = 33

cases only normal incidence is considered, i. e., $\theta_i = 0$. Figures 8 and 9 exhibit the comparisons for the y component of electric field along the x and y axes, respectively, for $a = \lambda/4$. Figures 10 and 11 exhibit the same comparisons for $a = \lambda/2$ and figures 12 and 13 show the comparisons for $a = 3\lambda/2$. For the radii $a = \lambda/4$ and $a = \lambda/2$ the numerical results and the measured data differ by no more than about 10%. However for $a = 3\lambda/2$ the agreement is not quite as good but this could be due to a convergence problem. On figures 8 through 13 the Kirchhoff approximation is presented (ref. 3). The Kirchhoff approximation for the aperture is equivalent to the physical optics approximation for the Babinet equivalent disk.

3. DIFFRACTED FIELD IN THE NEAR ZONE

As mentioned in the foregoing the electromagnetic field diffracted by a small aperture may be expressed in terms of the dipole moments of the magnetic source equivalent for the aperture field distribution. Although this procedure yields a simple formula for the diffracted field, the expression is not valid for the region very near the aperture (ref. 1). Using the numerical formulation that is presented, the diffracted field behind the aperture is calculated and compared to the dipole field approximation. Typical results are shown in figures 14 and 15 where the field components along the z axis are presented. One general observation is that the dipole expression is valid for distances from the aperture as small as the aperture radius.

As the frequency is increased until the aperture diameter becomes an appreciable fraction of a wavelength it must be expected that the dipole field

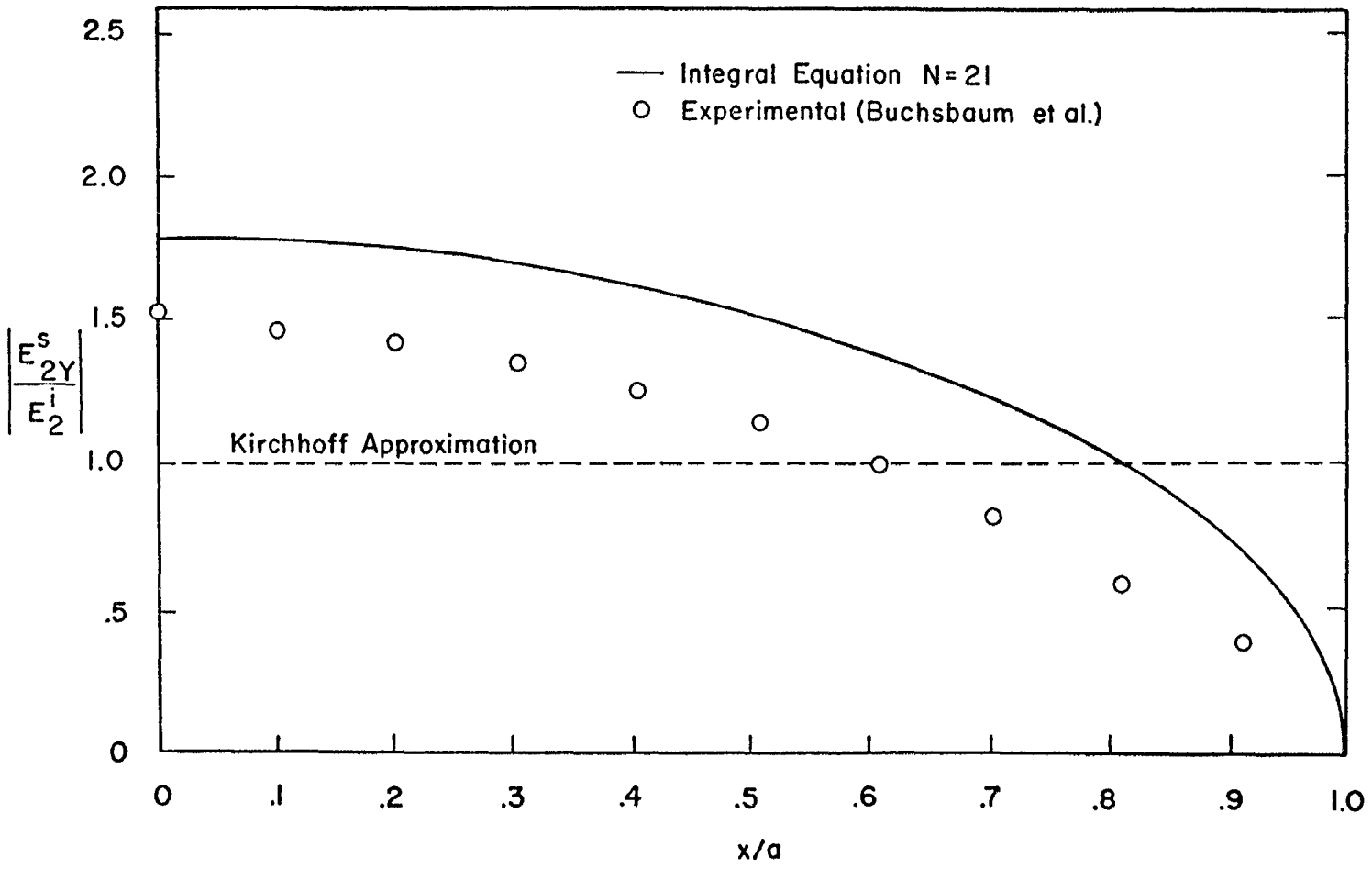

Figure 8. H-Plane Distribution of Electric Field Within an Aperture of .5λ in Diameter for Normal Incidence

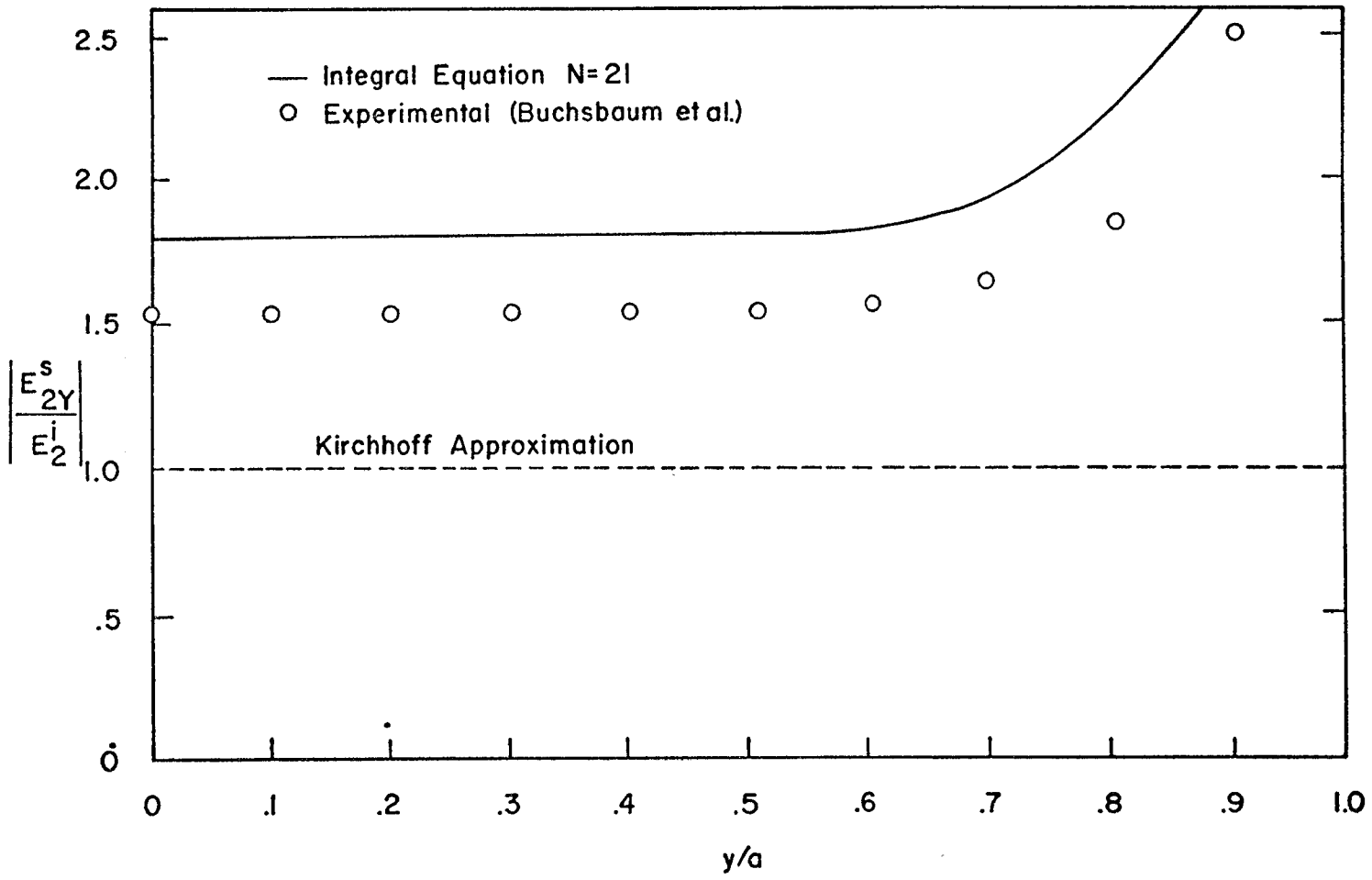

Figure 9. E-Plane Distribution of Electric Field Within an Aperture of .5λ in Diameter for Normal Incidence

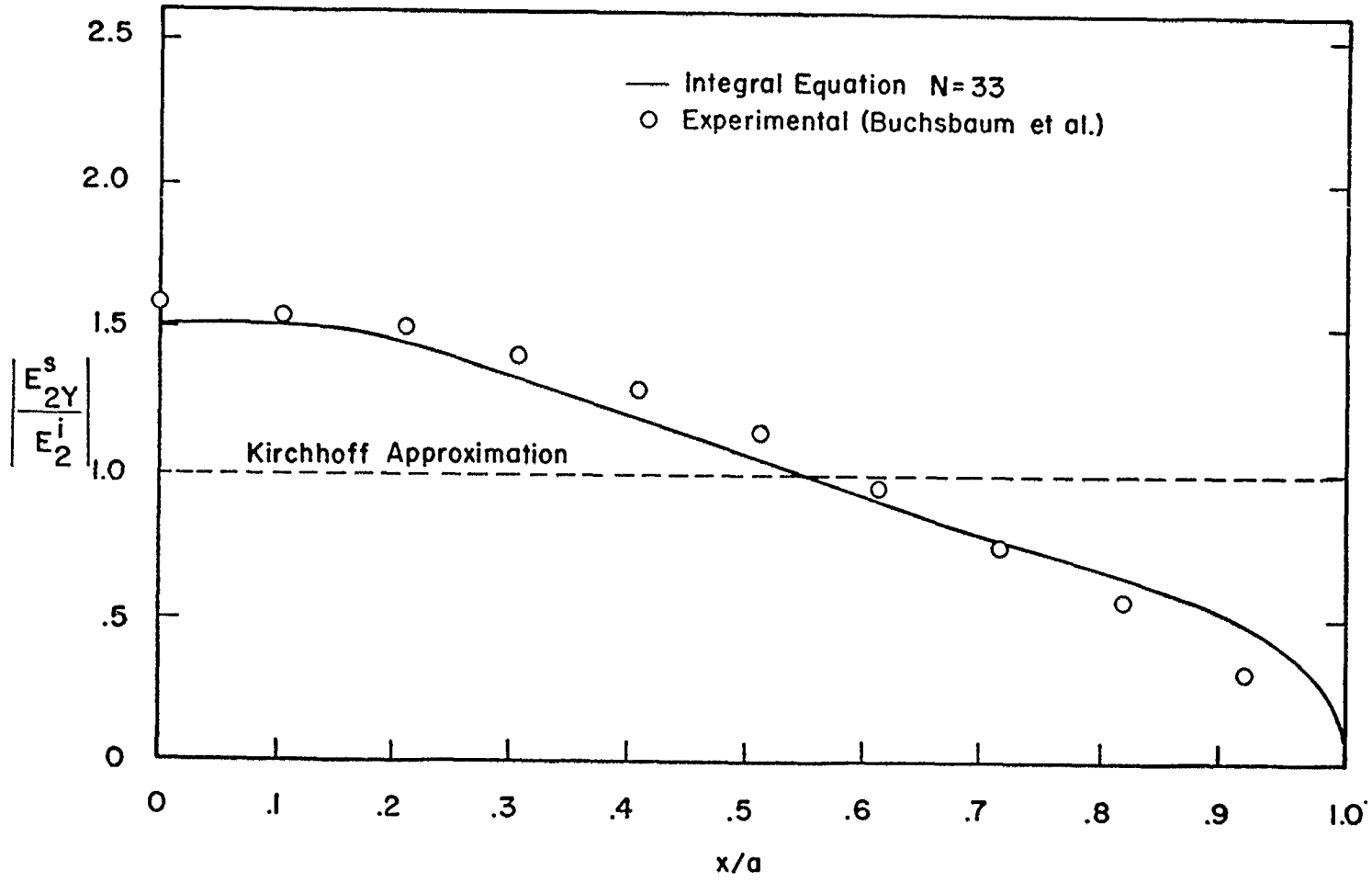

Figure 10. H-Plane Distribution of Electric Field Within Aperture of 1λ in Diameter for Normal Incidence

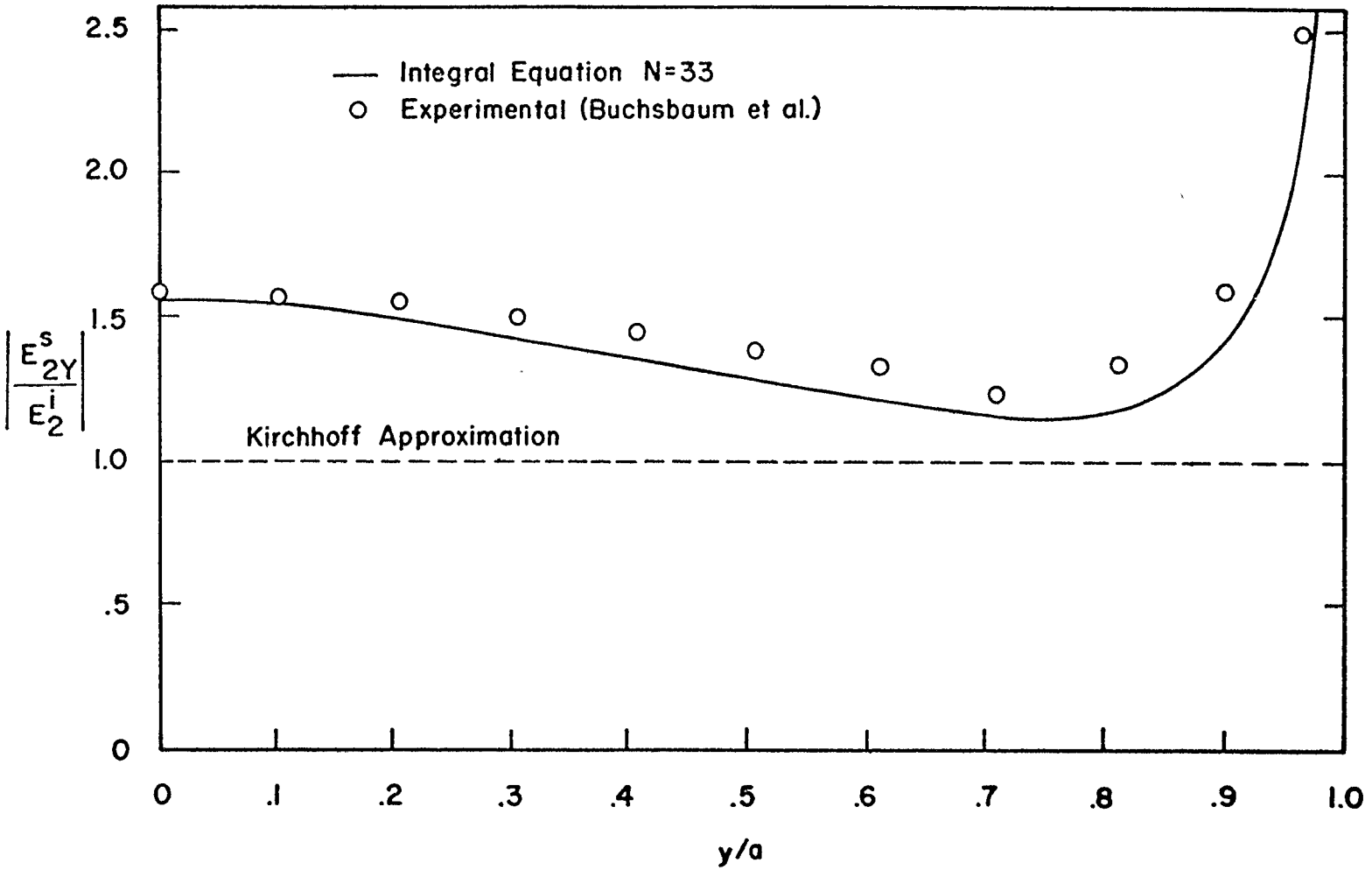

Figure 11. E-Plane Distribution of Electric Field Within an Aperture of 1λ in Diameter for Normal Incidence

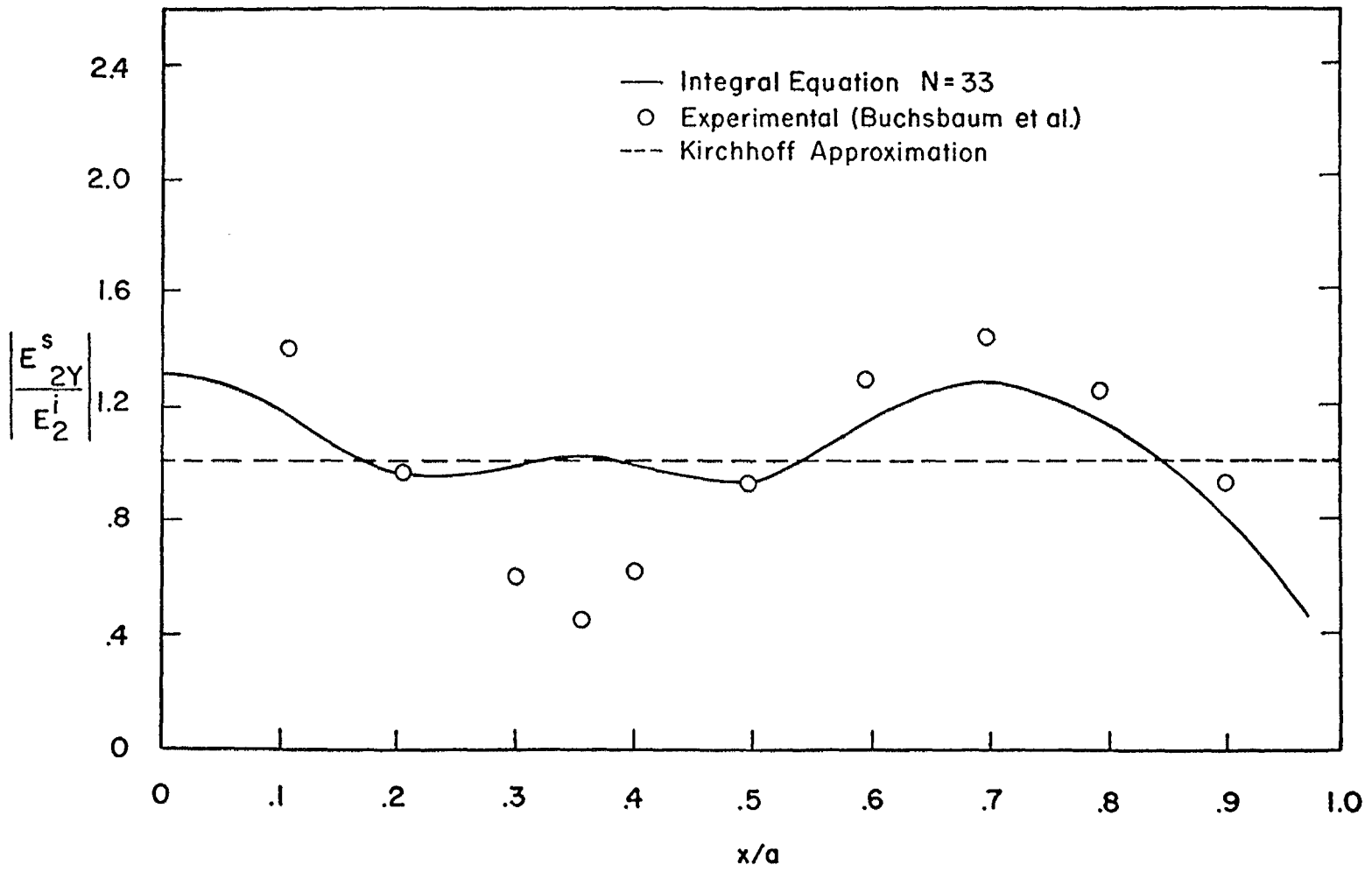

Figure 12. H-Plane Distribution of Electric Field Within an Aperture of 3λ in Diameter for Normal Incidence

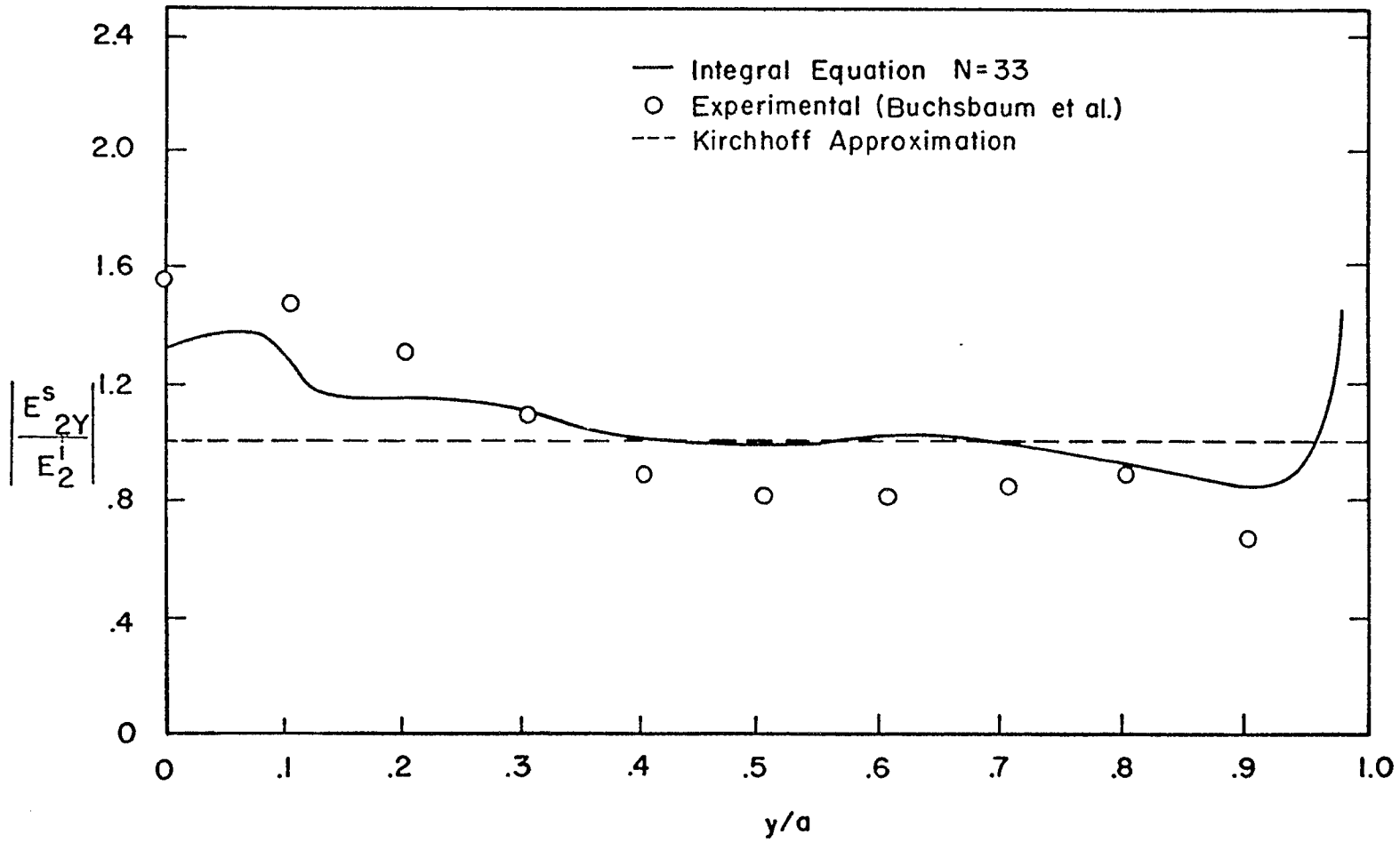

Figure 13. E-Plane Distribution of Electric Field Within an Aperture of 3λ in Diameter for Normal Incidence

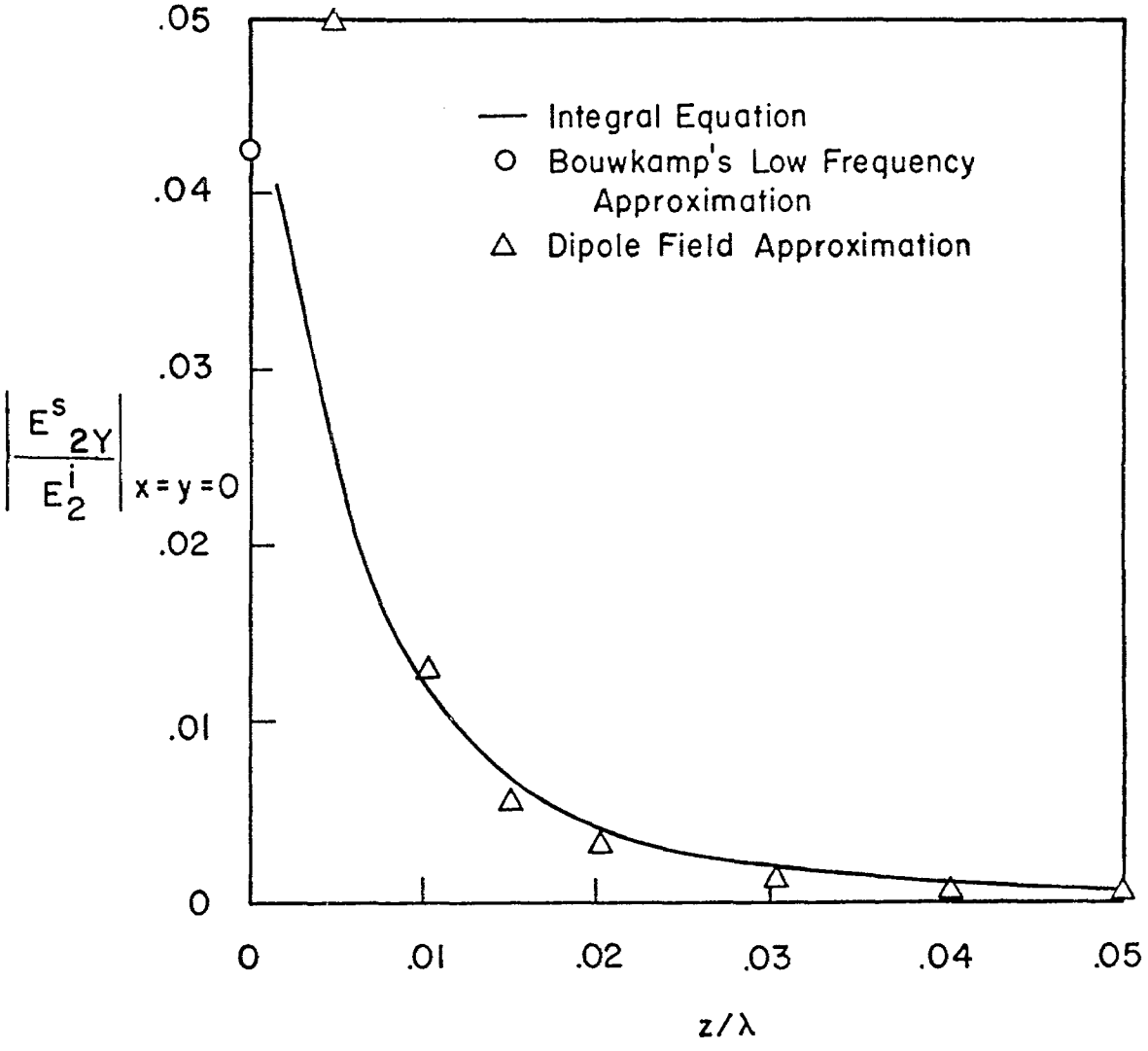

Figure 14. Distribution of Tangential Component of Scattered Electric Field for an Aperture of 0.0157λ in Diameter.

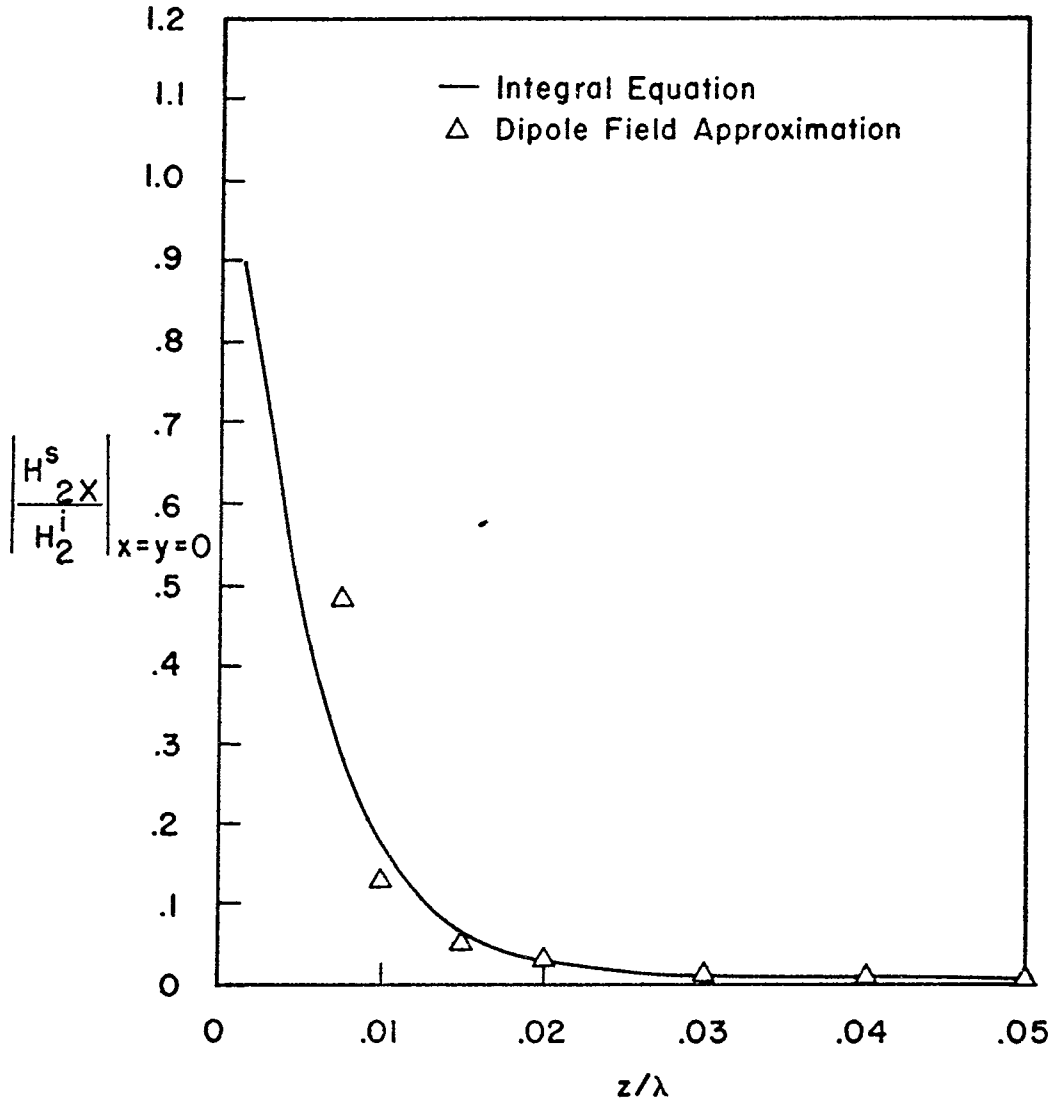

Figure 15. Distribution of the x Component of the Magnetic Field Penetrating an Aperture of 0.0157λ in Diameter for Normal Incidence

approximation would no longer be valid. However, from figures 16 and 17 it appears that the dipole field approximation yields reasonably good approximations for apertures with as large a radius as $a = \lambda/4$. Note that experimental results of Ehrlich, et. al. (ref. 16) are also shown in figure 16.

Experimental and theoretical results for the diffracted field along the z axis behind a circular aperture are shown in figures 18 and 19 for $a = \lambda/2$. Corresponding results for $a = 3\lambda/2$ are shown in figures 20 and 21. In all cases good agreement is obtained.

4. DIFFRACTED FIELD IN THE FAR ZONE

Since the diffracted field in the far zone is obtained using the same algorithms as the near zone it is expected to be of comparable accuracy or better. Figure 22 exhibits the far field along the z axis as obtained numerically and as obtained from the low and high frequency approximations. The low frequency approximation is based on the dipole field expression of ref. 1 and the high frequency approximation is based on the Kirchhoff approximation (ref. 3). For the data shown in figure 22 the radius of the aperture considered is not small enough for the low frequency approximation to be valid nor large enough for the high frequency approximation to be valid. Hence there are significant differences between the results of these approximations and the numerically obtained results. For a larger aperture, $a = \lambda/2$, the agreement between the high frequency approximation and the numerical results improves considerably as seen in figure 23. And when the aperture radius $a = 3\lambda/2$ (see figure 24) the Kirchhoff approximation data coincides with the numerical solution data. However, it must be expected that if the corresponding data were compared

---

16. Ehrlich, M. J., Silver, S., and Held, G., "Studies of the Diffraction of Electromagnetic Waves by Circular Apertures and Complementary Obstacles: The Near-Zone Field," Journal of Applied Physics, Vol. 26, No. 1, pp. 336-345, March 1955.

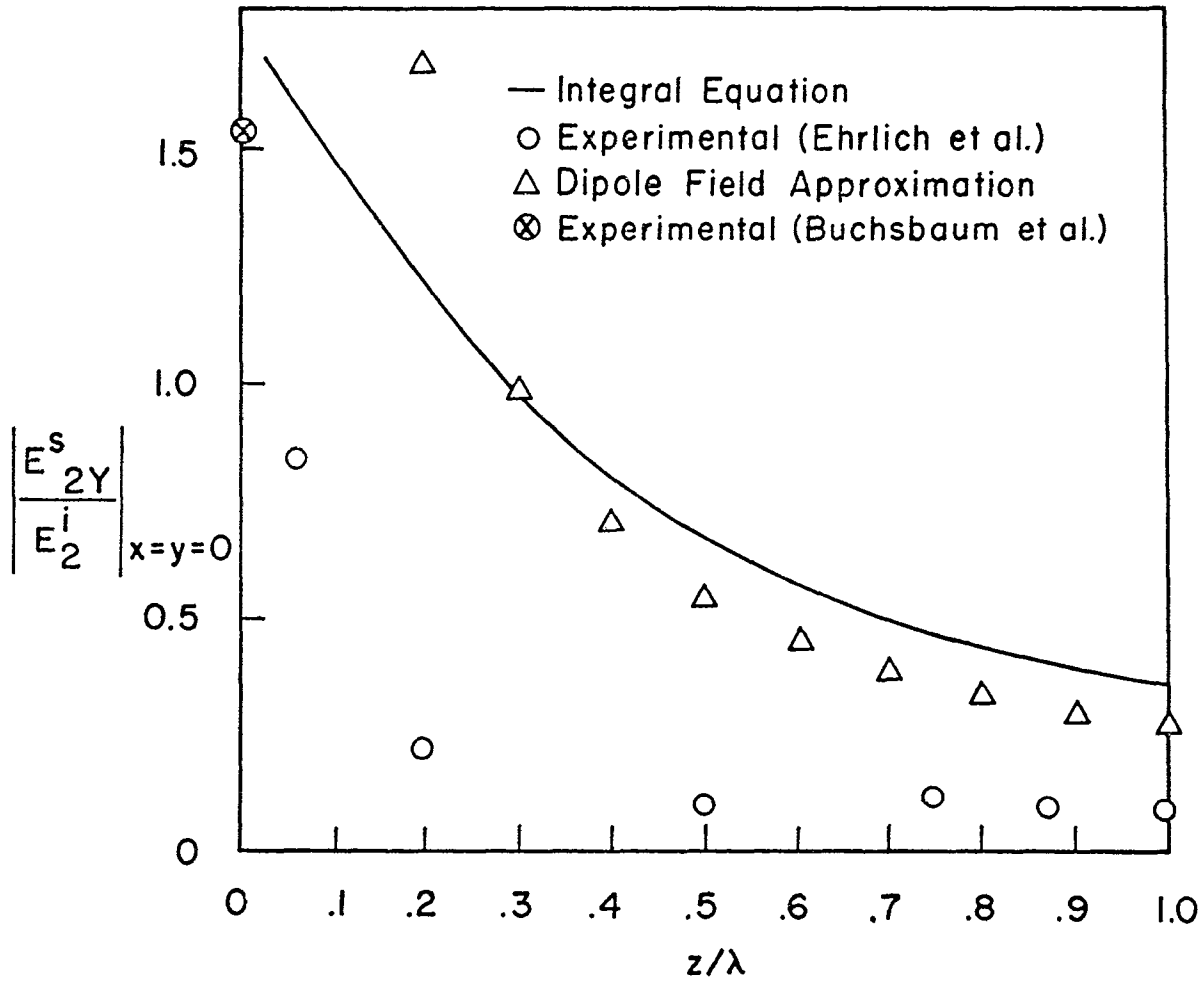

Figure 16. Distribution of the y Component of the Electric Field Penetrating an Aperture of 0.5λ in Diameter for Normal Incidence

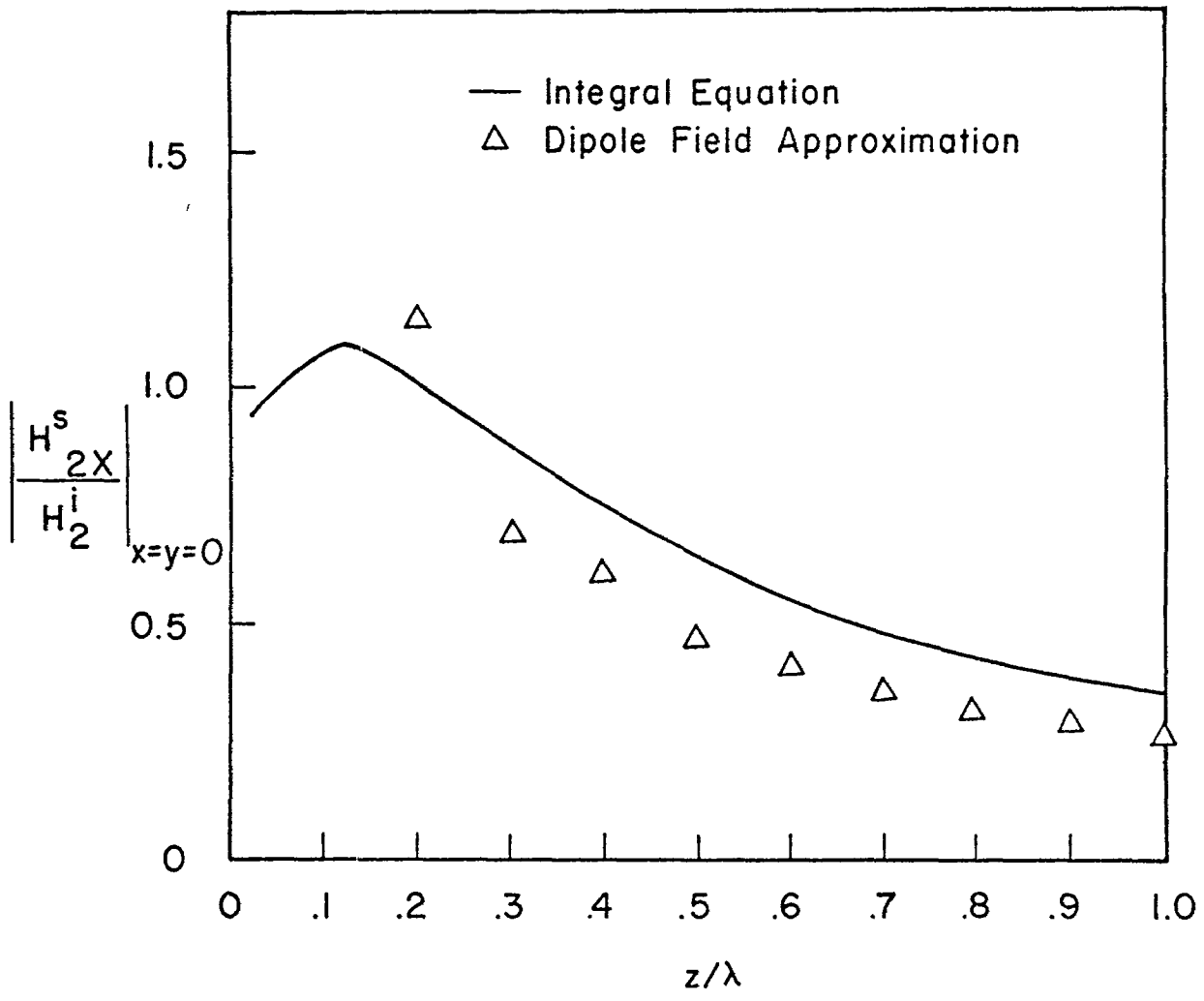

Figure 17. Distribution of the x Component of the Magnetic Field Penetrating an Aperture of 0.5λ in Diameter for Normal Incidence.

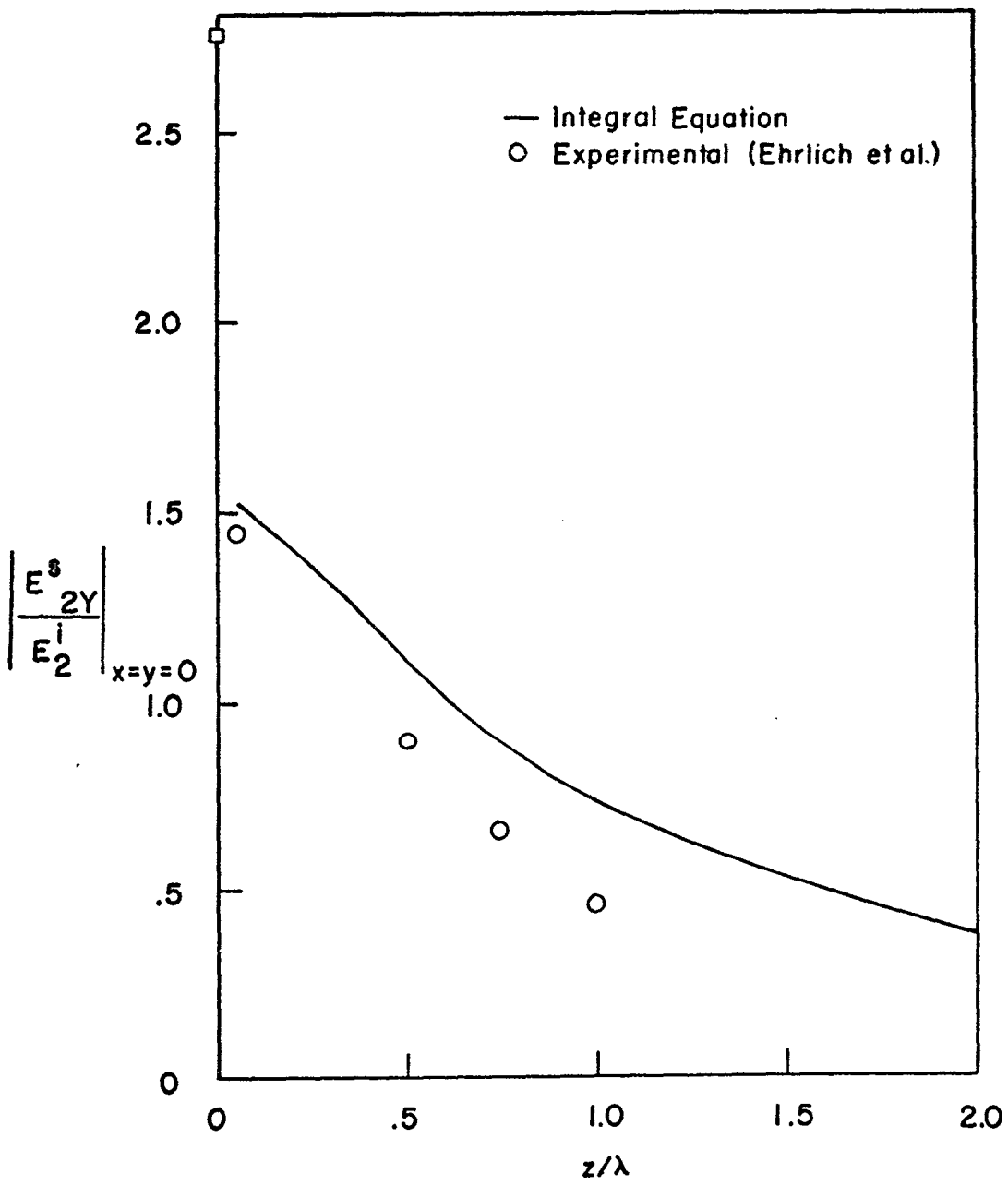

Figure 18. Distribution of the y Componenet of the Electric Field Penetrating an Aperture of 1.0λ in Diameter for Normal Incidence

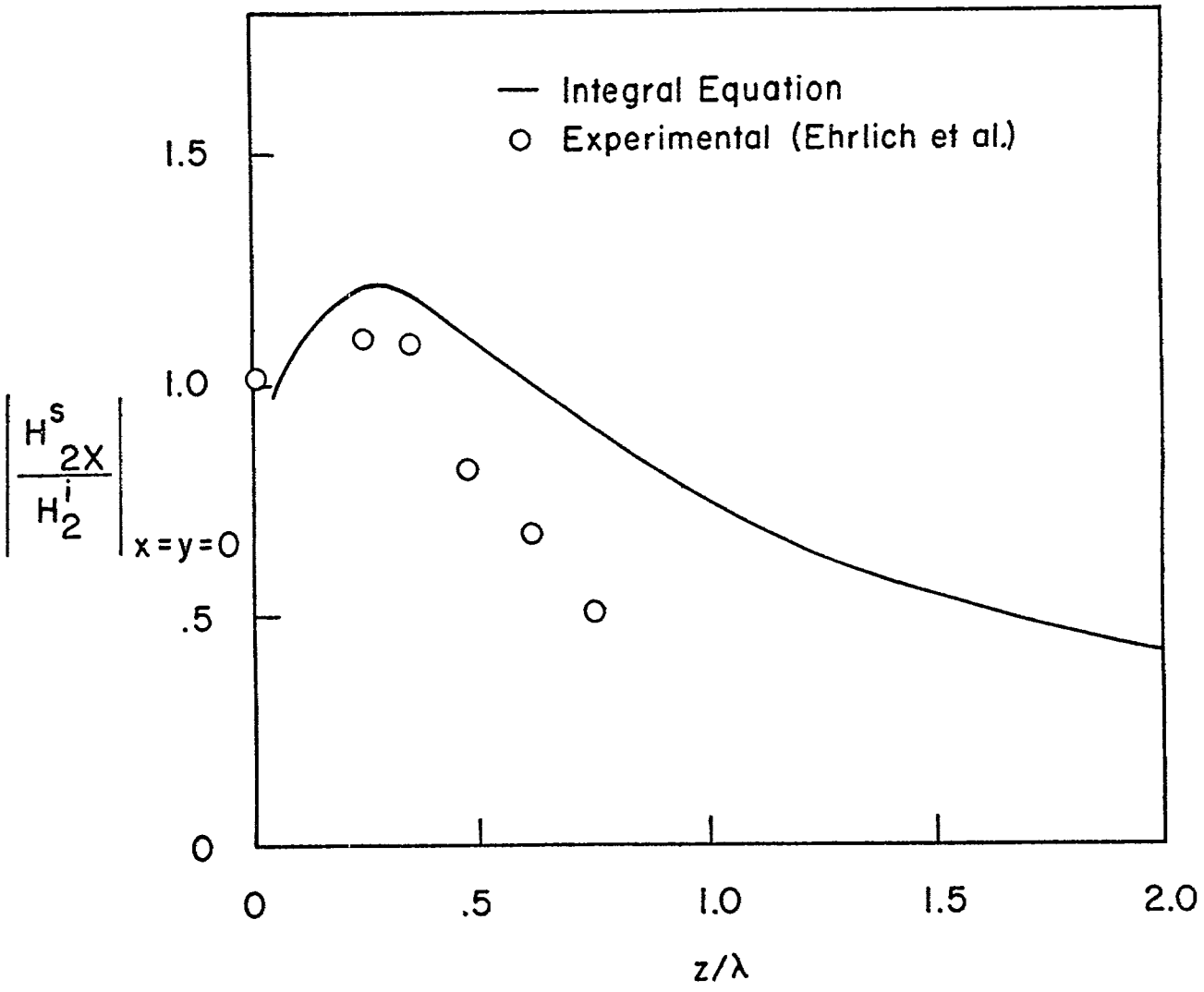

Figure 19. Distribution of the x Component of the Magnetic Field Penetrating an Aperture of 1.0λ in Diameter for Normal Incidence

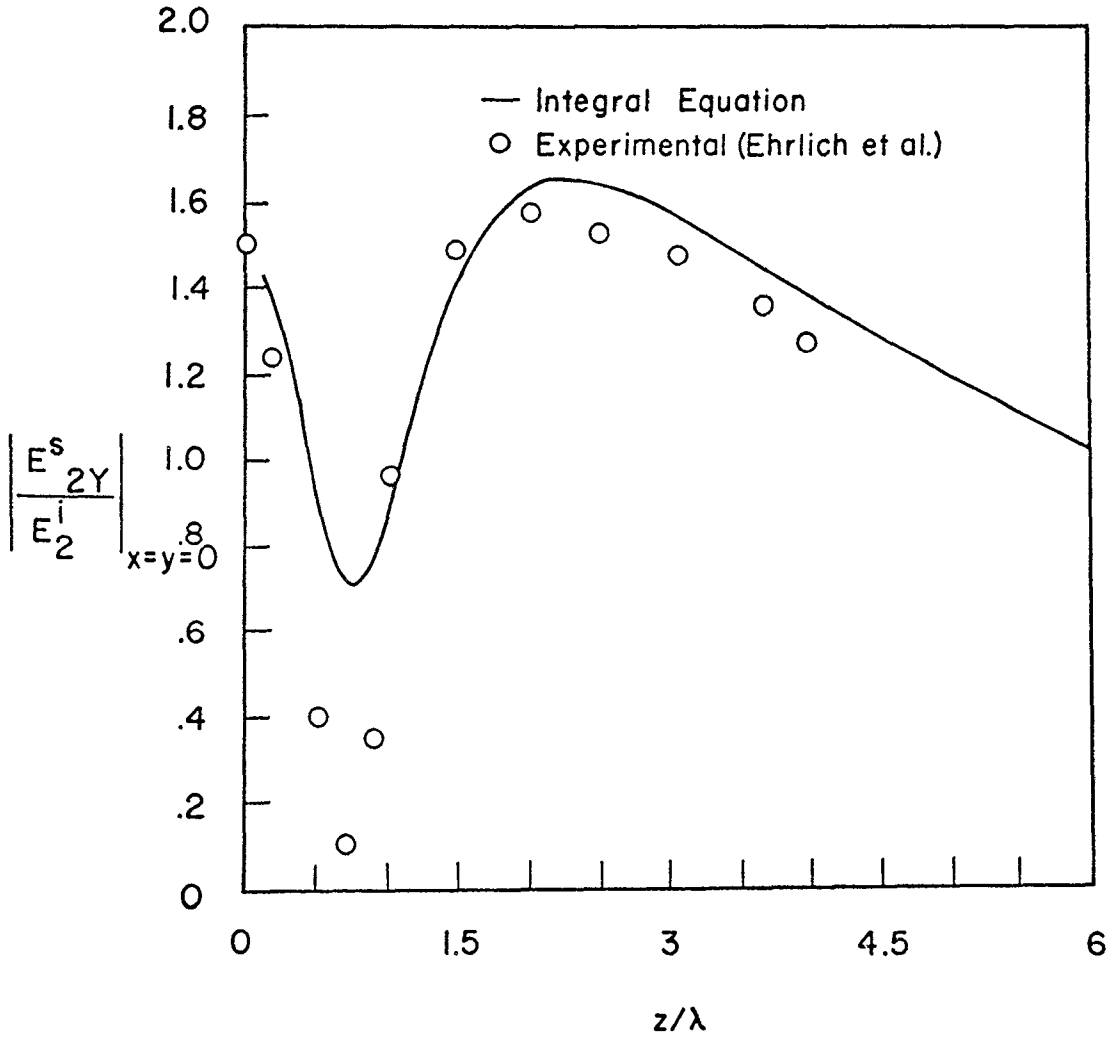

Figure 20. Distribution of the y Component of the Electric Field Penetrating an Aperture of 3.0λ in Diameter for Normal Incidence

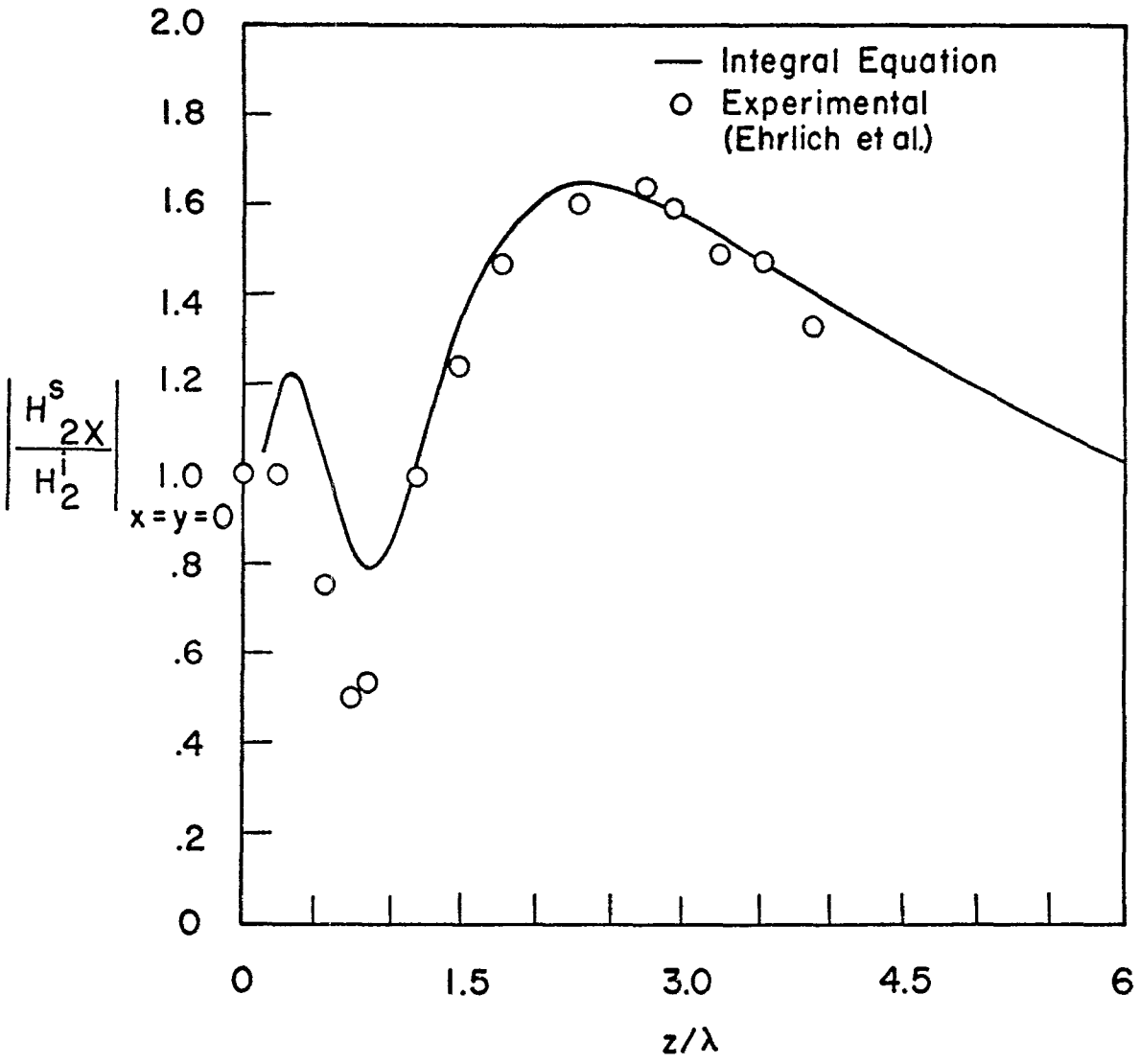

Figure 21. Distribution of the x Component of the Magnetic Field Penetrating an Aperture of 3.0λ in Diameter for Normal Incidence.

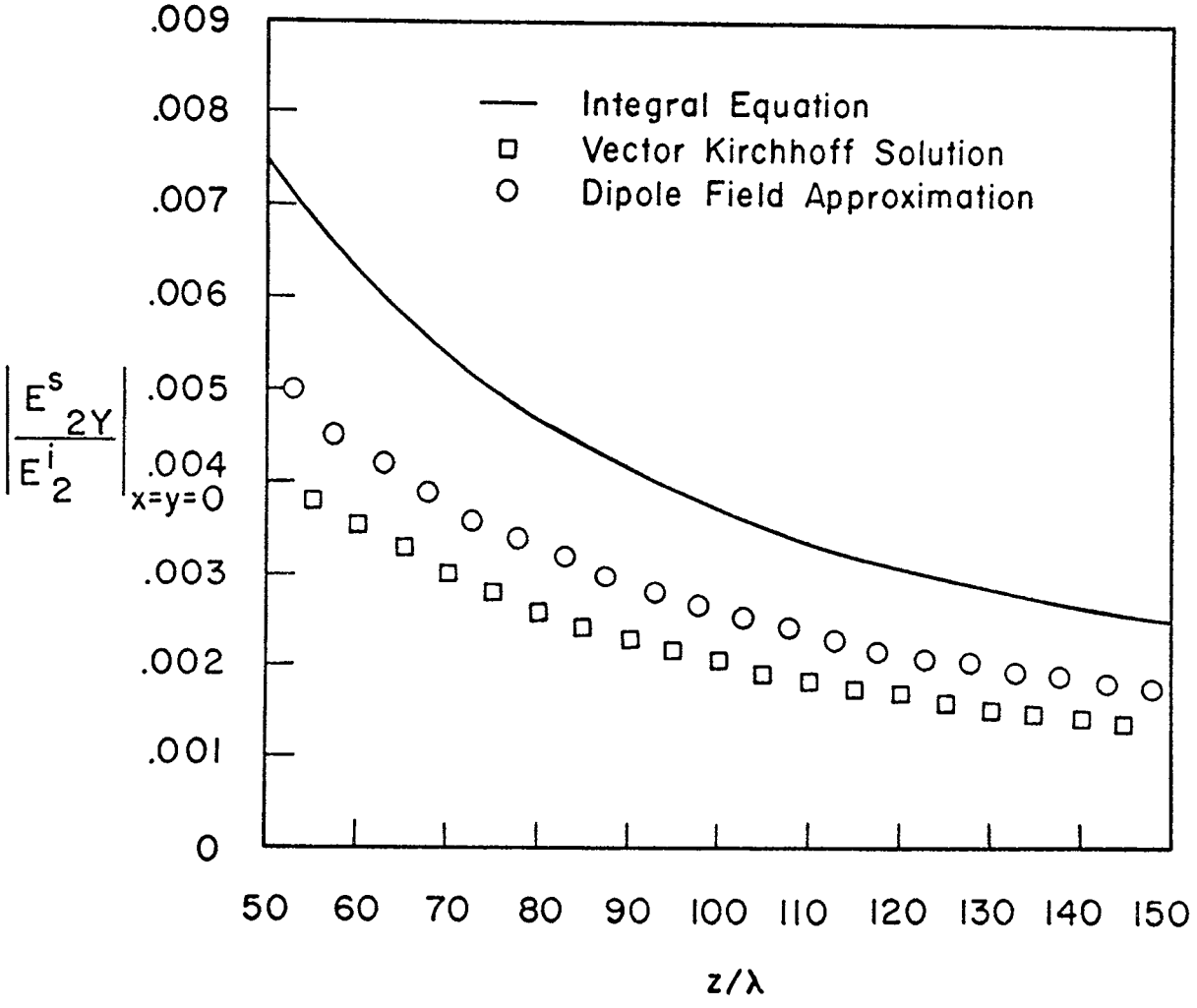

Figure 22. Distribution of the y Component of the Electric Field Penetrating an Aperture of 0.5λ Diameter for Normal Incidence

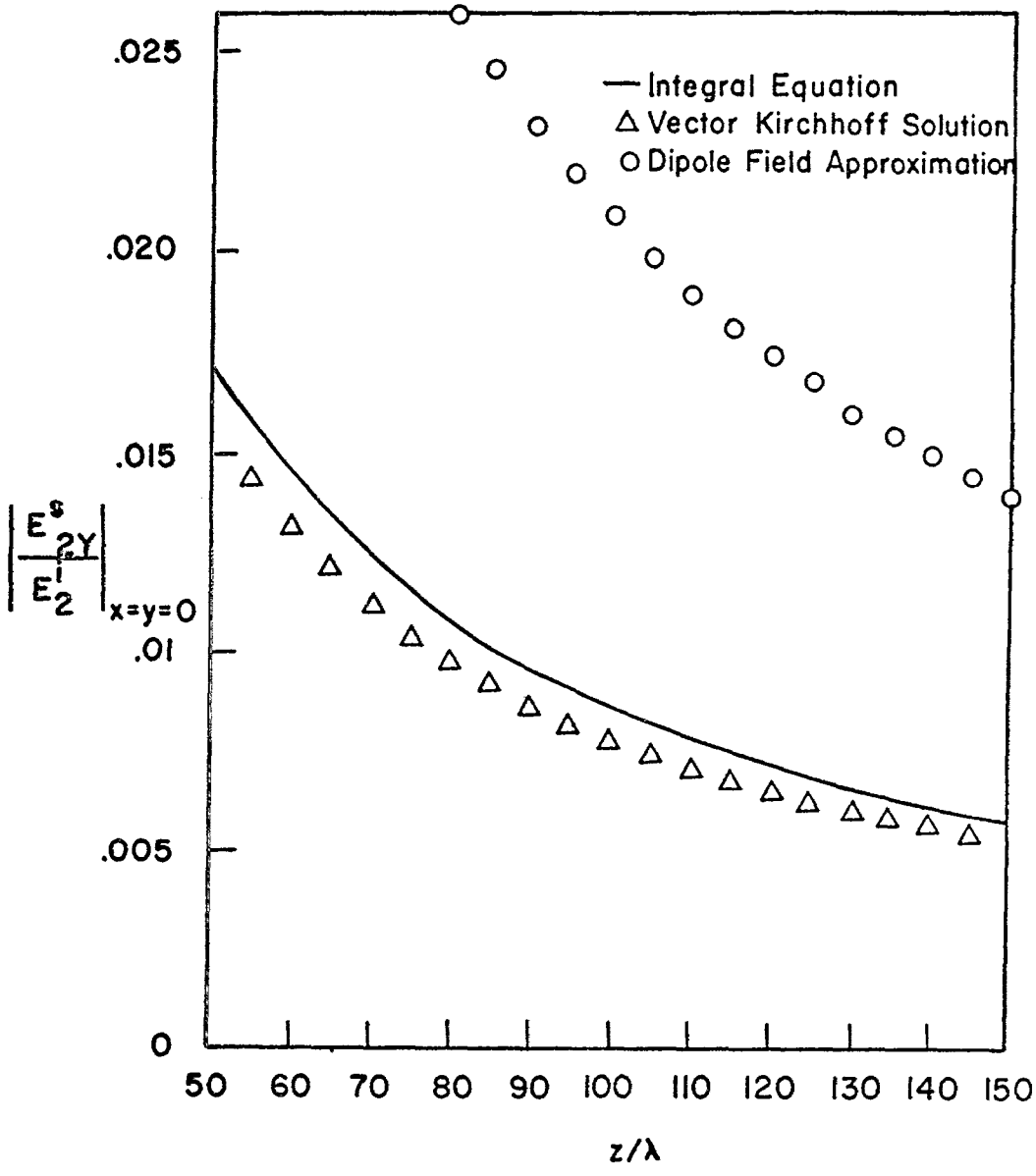

Figure 23. Distribution of the y Component of the Electric Field Penetrating an Aperture of 1.0λ Diameter for Normal Incidence

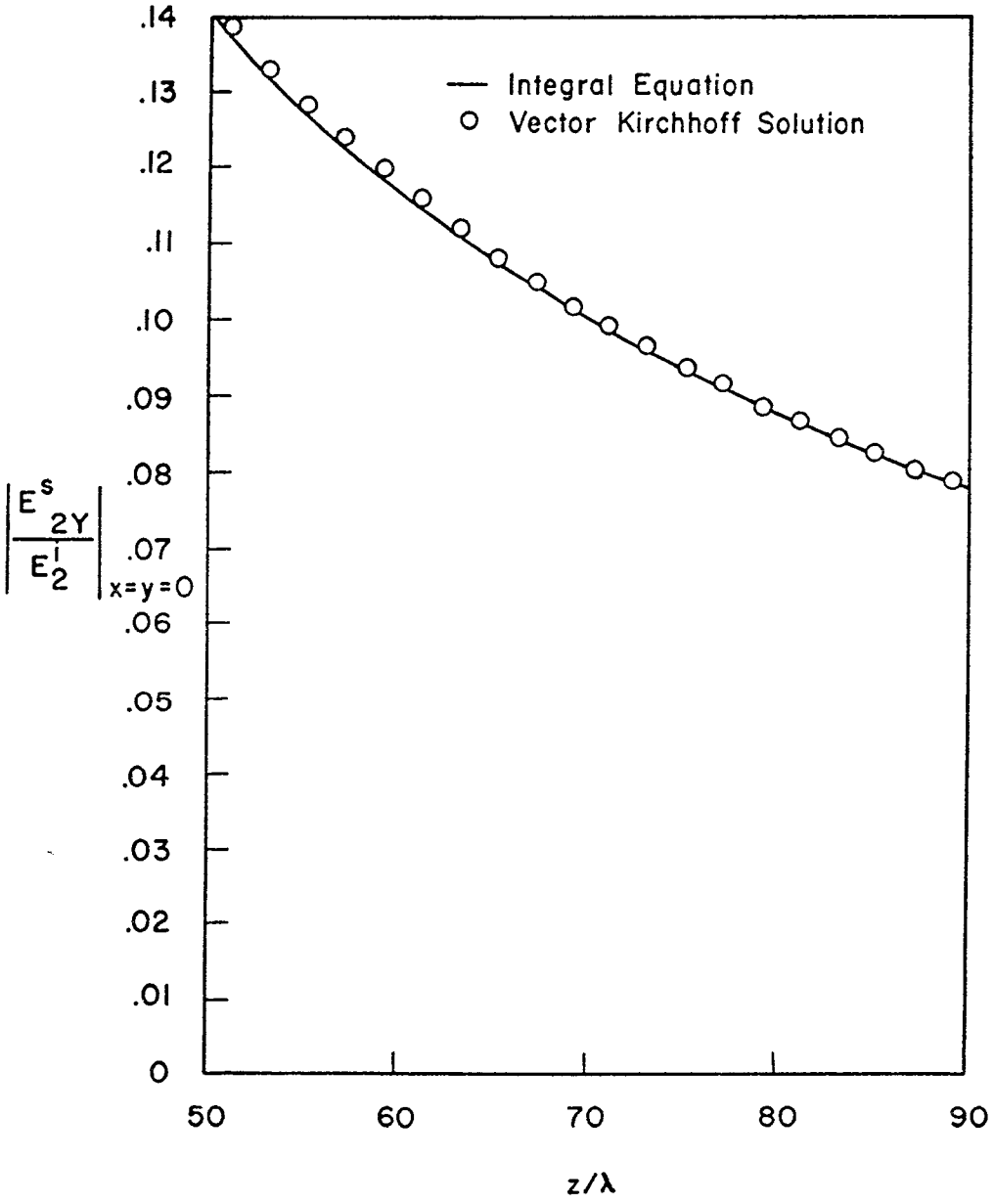

Figure 24. Distribution of the y Component of the Electric Field Penetrating an Aperture of 3.0λ Diameter for Normal Incidence

for points off the z axis then the agreement would not be as good since the Kirchhoff approximation would not adequately approximate the aperture field distribution.

5. SINGULARITY EXPANSION RESULTS

To apply the singularity expansion method it is first necessary to perform a pole search on the S matrix. The numerical search is time consuming; therefore, only a small number of current zones are used and only one or two poles are located for several modes. For the details of the computational procedures see ref. 17. Table 2 gives the pole locations, s_{mj}, for several m values. Table 3 is a study of the pole location as the number of current zones is varied. It is noted that in most cases the real part of the poles are much less than the imaginary part. Probably these data are not correct. Furthermore it is found that substantial variation in the real part of the poles may occur and yet the poles still satisfy the numerical criteria used by the computer program in identifying poles. Evidently this subject requires further investigation. However, the imaginary parts of the poles appear quite reasonable and are possibly correct.

Following the numerical techniques described in ref. 17 the coupling vectors, the residue matrix and coupling coefficients may be determined. Figures 24 and 25 show the real part of the mode vectors corresponding to J_r and J_ϕ, respectively, for the poles presented in Table 2. Also shown in figure 26 is the real part of the electric and magnetic field natural mode vector for the s_{11} and s_{12} poles.

---

17. Crow, T. T., Graves, B. D., and Taylor, C. D., "Numerical Techniques Useful in the Singularity Expansion Method as Applied to Electromagnetic Interaction Problems, AFWL Mathematics Note 27, December 1972.

TABLE 2. NATURAL FREQUENCIES FOR THE DISK

Mode	S_{mj}	$\sigma a/c$	$\omega a/c$
0	S_{01}	-1.093	3.905
1	S_{11}	-.00048	1.378
1	S_{12}	-.00072	3.575
2	S_{21}	-.00021	2.624

TABLE 3. S_{11} VS. NUMBER OF CURRENT ZONES

N	$\sigma a/c$	$\omega a/c$
6	-.00048	1.378
8	-.000056	1.405
10	-.000081	1.419
12	-.0000054	1.424

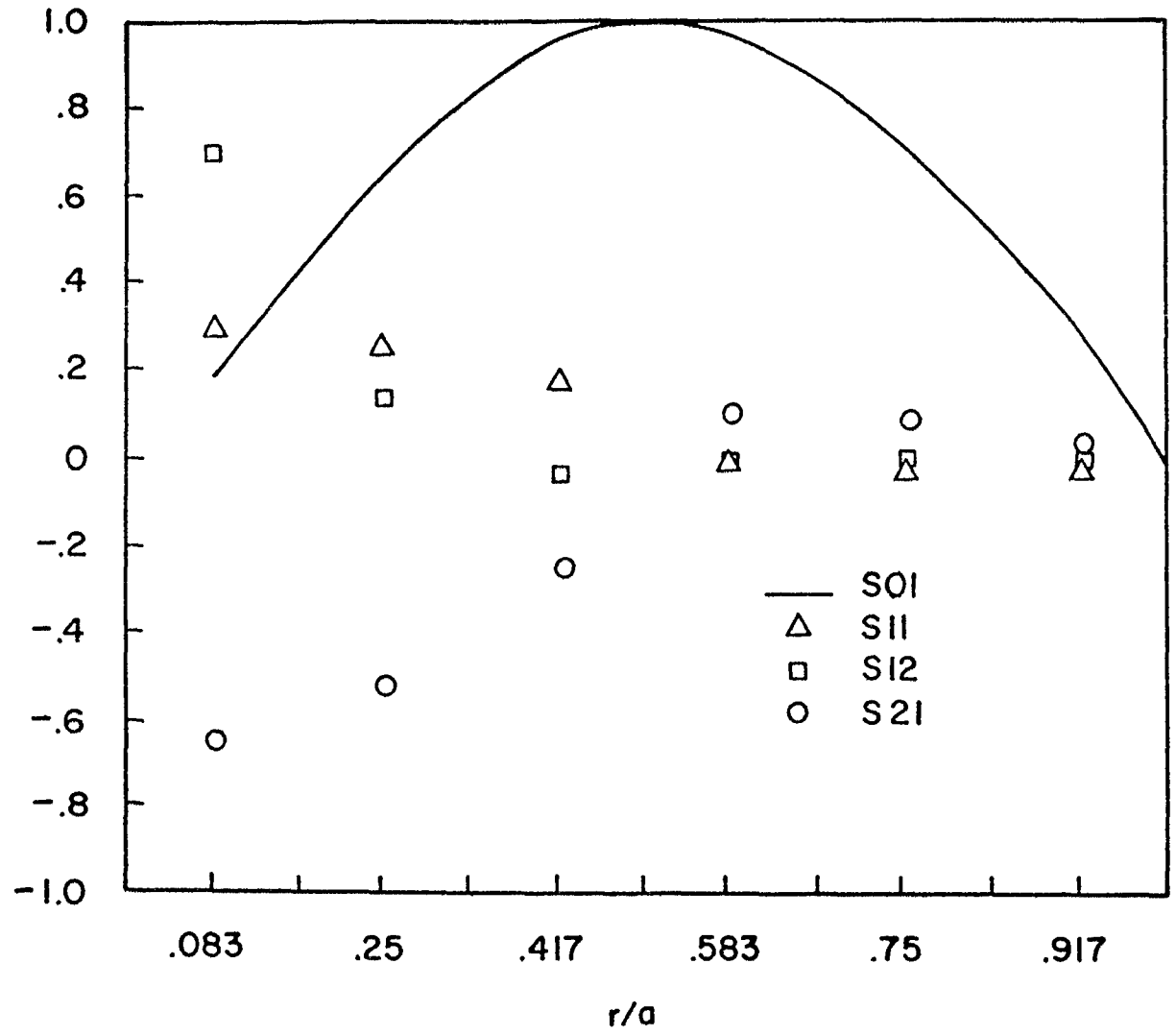

Figure 25. Real Part of Mode Vectors Corresponding to J_r

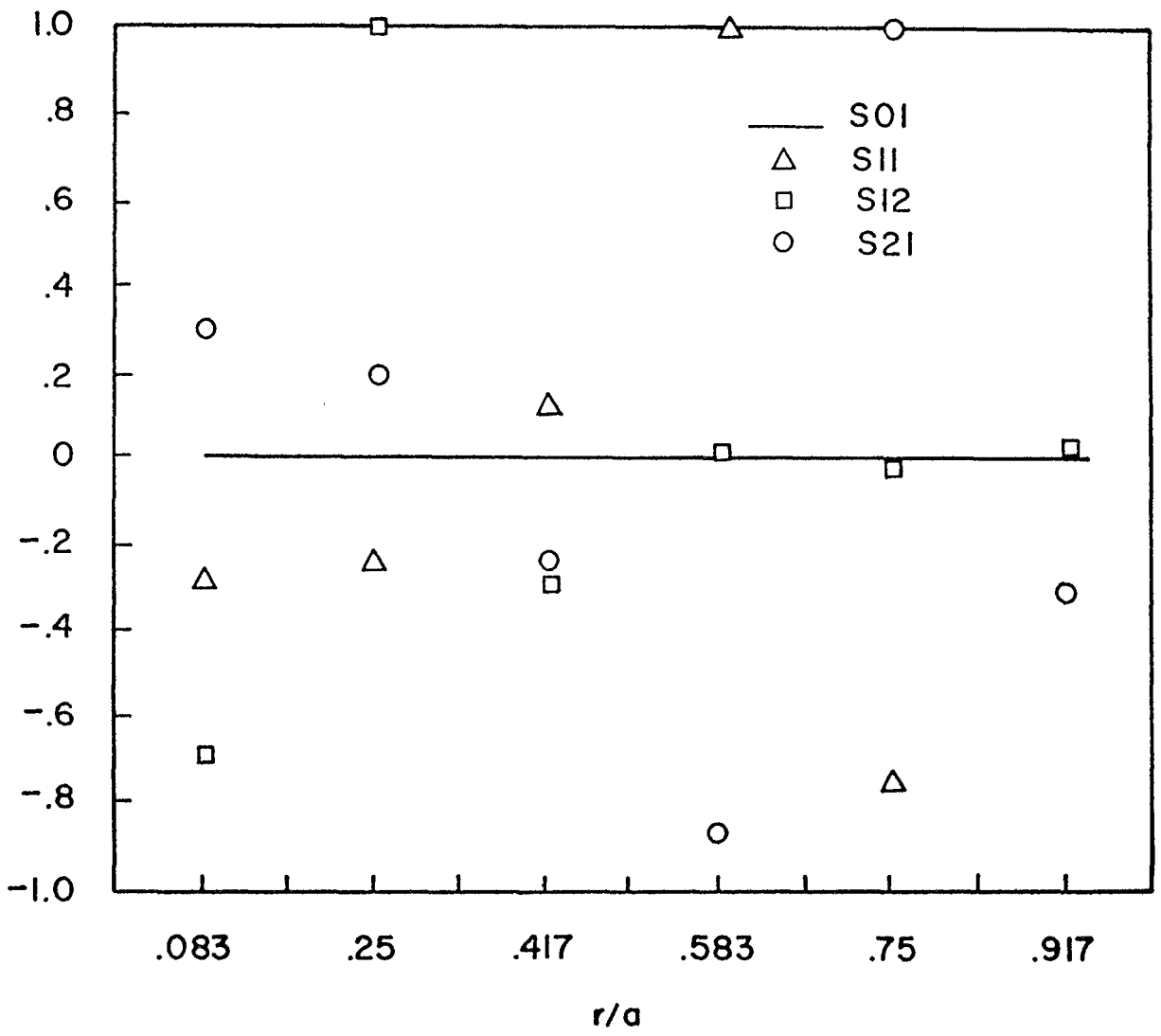

Figure 26. Real Part of Mode Vectors Corresponding to J_ϕ

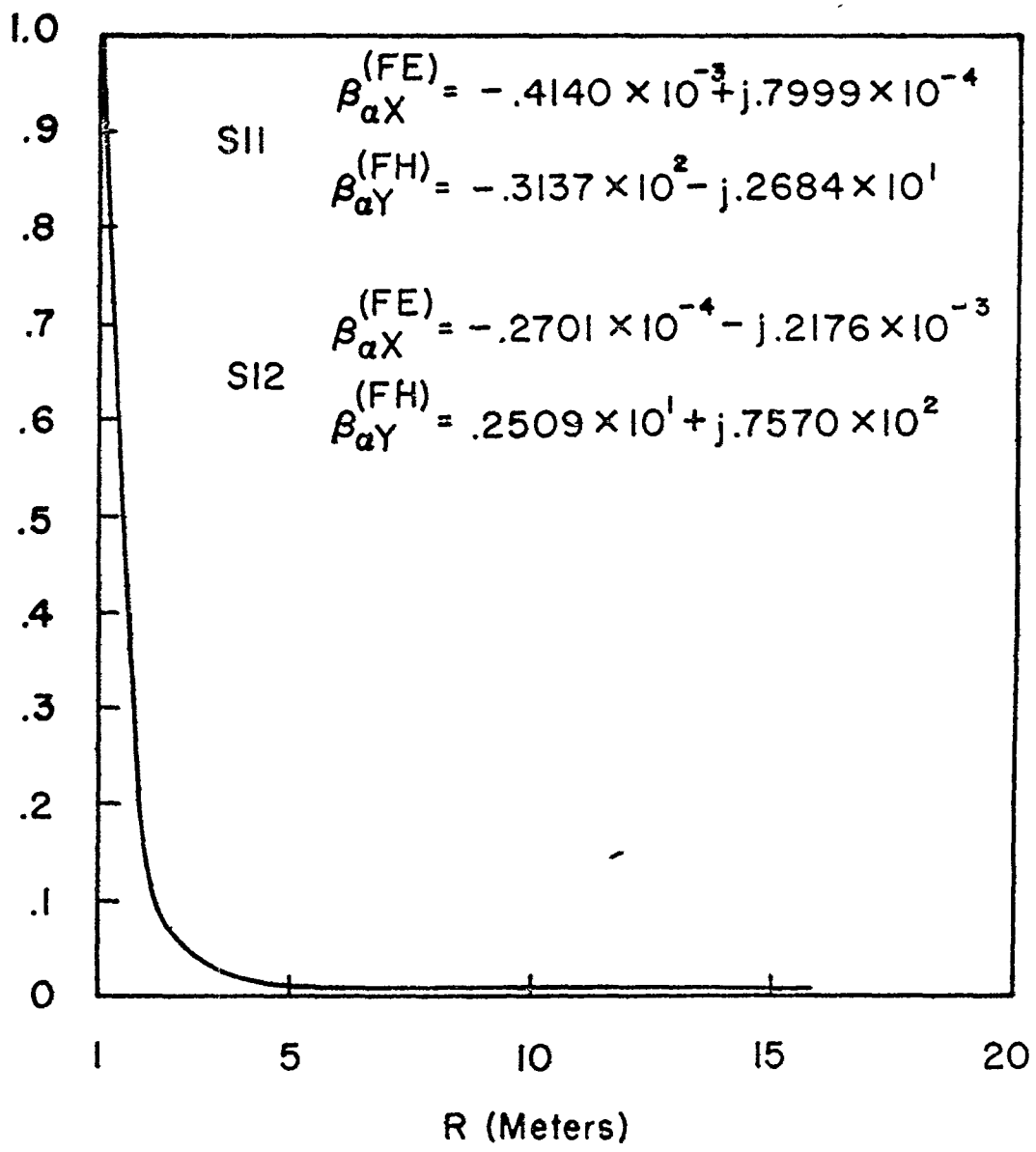

Figure 27. Real Part of Electric and Magnetic Fields Natural Mode Vector Corresponding to Poles S11 and S12.

6. CAVITY BACKED APERTURES

Perhaps the simplest cavity backed aperture for studying purposes is formed by placing an infinite conducting plate behind a plate containing an aperture. If the field attenuates sufficiently with distance from the aperture then the presence of the second plate may be ignored. This would be a valid approximation for electrically small apertures when the plate spacing is large compared to the aperture radius (see figures 14 and 15). Under the same condition of plate spacing figures 16 through 19 indicate the presence of the second plate may be ignored for aperture radii as large as $\lambda/2$. For larger aperture radii the Kirchhoff approximation could be used to advantage together with imaging techniques such as is discussed in ref. 1.

SECTION IV

CONCLUSIONS

A numerical solution to the problem of the electromagnetic field penetration through apertures is possible. The solution technique in principle is not frequency limited; however, practical considerations limit the technique to treating apertures with radii less than a few wavelengths. Several observations are made concerning the low frequency and high frequency approximate solutions.

1. In the low frequency regime the dipole approximation for the diffracted field is valid for distances from the aperture greater than the aperture radius. This result is of interest in many problems.[18]

2. In the high frequency regime the Kirchhoff approximation becomes valid when the aperture radius is greater than a few wavelengths.

3. The near field behind an aperture decreases rapidly with distance from the aperture at low frequency. However at high frequency this does not occur.

4. The far field behind an aperture is predicted accurately by the dipole approximation for frequencies up to the first resonant frequency of the aperture. And the Kirchhoff approximation yields very accurate far field predictions whenever the aperture radius is greater than a few wavelengths.

---

[18]Latham, R. W., "Small Holes in Cable Shields," AFWL Interaction Note 118, September 1972.

REFERENCES

1. Taylor, C. D., "Electromagnetic Pulse Penetration Through Small Apertures," AFWL Interaction Note 74, March 1971.

2. Bethe, H. A., "Theory of Diffraction by Small Holes," Phys. Rev., Vol. 66, pp. 163-182, October 1944.

3. Jones, D. S., The Theory of Electromagnetism, Pergamon Press, New York, 1964, pp. 626-640.

4. Flammer, C., "The Vector Wave Function Solution of the Diffraction of Electromagnetic Waves by Circular Disks and Apertures. II. The Diffraction Problems," J. Appl. Phys., Vol. 24, No. 9, pp. 1224-1231, September 1953.

5. Andreason, M. G., "Scattering from Bodies of Revolution," IEEE Trans. Ant. and Prop., Vol. AP-13, pp. 303-310, March 1965.

6. Baum, C. E. "On the Singularity Expansion Method for the Solution of Electromagnetic Interaction Problems," AFWL Interaction Note 88, December 1971.

7. Harrington, R. F., Field Computation by Moment Methods, The MacMillan Company, New York, 1968.

8. Meixner, V. J. and Andrejewski, W., "Strenge Theorie der Beugung ebener elektromagnetischer Wellen an der Vollkommen leitenden Kreisscheibe und an der kreisformigen Offnung im vollkommen leitenden ebenen Schirm," Annalen der Physik, Band 7, pp. 157-168, 1950.

9. Abramowitz, M. and Stegun, I. A., editors, Handbook of Mathematical Functions, Dover Publications, Inc., New York, 1965, p. 591.

10. Edwards, J., Treatise on Integral Calculus, Vol. 1, Chelsea Publishing Co., New York, 1954, pp. 340-349.

11. Stratton, J. A., Electromagnetic Theory, McGraw-Hill Book Company, New York, 1941, pp. 371-372.

12. Crow, T. T., Graves, B. D. and Taylor, C. D., "The Singularity Expansion Method as Applied to Perpendicular Crossed Cylinders in Free Space," AFWL Interaction Note 161, October 1973.

13. Bouwkamp, C. J., "Diffraction Theory," Rep. Progr. Phys., 17, pp. 35-100, 1954.

14. Harrington, R. F., Time Harmonic Electromagnetic Fields, McGraw-Hill Book Company, New York, 1961, pp. 127-128.

15. Buchsbaum, S. J., Milne, A. R., Hogg, D. C., Bekefi, G. and Woonton, G. A., "Microwave Diffraction by Apertures of Various Shapes," J. Appl. Phys., Vol. 26, pp. 706-715, June 1955.

16. Ehrlich, M. J., Silver, S., and Held, G., "Studies of the Diffraction of Electromagnetic Waves by Circular Apertures and Complementary Obstacles; The Near-Zone Field," Journal of Applied Physics, Vol. 26, No. 1, pp. 336-345, March 1955.

17. Crow, T. T., Graves, B. D., and Taylor, C. D., "Numerical Techniques Useful in the Singularity Expansion Method as Applied to Electromagnetic Interaction Problems, AFWL Mathematics Note 27, December 1972.

18. Latham, R. W., "Small Holes in Cable Shields," AFWL Interaction Note 118, September 1972.